The mechanical regulation of RNA binding protein hnRNPC in the failing heart

Fabiana Martino[1,2,3*], Nandan Mysore Varadarajan[4], Ana Rubina Perestrelo[1], Vaclav Hejret[4,5], Helena Durikova[1], Vladimir Horvath[1,6], Francesca Cavalieri[7,8], Frank Caruso[7], Waleed S. Albihlal[9], André P. Gerber[9], Mary A. O'Connell[4], Stepanka Vanacova[4], Stefania Pagliari[#1,3], Giancarlo Forte[#1,3].

[1]International Clinical Research Center (ICRC) of St Anne's University Hospital, CZ-65691 Brno, Czech Republic; [2]Faculty of Medicine, Department of Biology, Masaryk University, CZ-62500 Brno, Czech Republic; [3]Competence Center for Mechanobiology in Regenerative Medicine, INTERREG ATCZ133, CZ-62500 Brno, Czech Republic;[4]Central European Institute of Technology (CEITEC), Masaryk University; [5]National Centre for Biomolecular Research, Masaryk University, Brno, Czech Republic; [6]Centre for Cardiovascular and Transplant Surgery, Brno, Czech Republic; [7]ARC Centre of Excellence in Convergent Bio-Nano Science and Technology, and the Department of Chemical Engineering, The University of Melbourne, Parkville, Victoria 3010, Australia; [8]Dipartimento di Scienze e Tecnologie Chimiche, Università degli Studi di Roma Tor Vergata, via della Ricerca Scientifica 1, 00133, Rome, Italy; [9]Dept. Microbial Sciences, Faculty of Health and Medical Sciences, University of Surrey, Guildford GU2 7XH, United Kingdom.

** current address: National Heart and Lung Institute, Imperial College London, London, United Kingdom.*

Running title: mechanosensitive hnRNPC in heart failure.

[#]These authors contributed equally to the study

Corresponding authors:

Giancarlo Forte, PhD
Center for Translational Medicine (CTM)
International Clinical Research Center (ICRC)
St. Anne's University Hospital
Studentska 6, Brno
Czech Republic, 62500
Tel: +420-543185449
giancarlo.forte@fnusa.cz

Stefania Pagliari, PhD
Center for Translational Medicine (CTM)
International Clinical Research Center (ICRC)
St. Anne's University Hospital
Studentska 6, Brno
Czech Republic, 62500
Tel: +420-543185449
stefania.pagliari@fnusa.cz

ABSTRACT

Cardiac pathologies are characterized by intense remodeling of the extracellular matrix (ECM) that eventually leads to heart failure. Cardiomyocytes respond to the ensuing biomechanical stress by re-expressing fetal contractile proteins via transcriptional and post-transcriptional processes, like alternative splicing (AS). Here, we demonstrate that the heterogeneous nuclear ribonucleoprotein C (hnRNPC) is upregulated and relocates to the sarcomeric Z-disk upon ECM pathological remodeling. We show that this is an active site of localized translation, where the ribonucleoprotein associates to the translation machinery. Alterations in hnRNPC expression and localization can be mechanically determined and affect the AS of numerous mRNAs involved in mechanotransduction and cardiovascular diseases, like Hippo pathway effector YAP1. We propose that cardiac ECM remodeling serves as a switch in RNA metabolism by impacting an associated regulatory protein of the spliceosome apparatus. These findings offer new insights on the mechanism of mRNAs homeostasis mechanoregulation in pathological conditions.

KEYWORDS

Heart failure; alternative splicing; mechanotransduction; RNA-binding proteins; hnRNPC.

48 **INTRODUCTION**

49 The onset and progression of aging-associated pathologies is paralleled by continuous local
50 extracellular matrix (ECM) remodeling. This remodeling serves as a compensatory strategy for
51 tissues to cope with altered conditions [1]. ECM remodeling is perceived and transmitted within a
52 cell through the modulation of cytoskeleton-propagated intracellular tension [2] that eventually
53 affects tissue-specific cell responses and function [3,4]. Cardiac pathologies are a prime example of
54 how ECM remodeling can impact on cell functionality, here affecting muscle contractility and
55 organ pumping [5]. Independently of the etiology, cardiac remodeling confers a major shift in
56 cardiomyocyte contractile function by inducing changes in signaling axes [6], metabolic pathways [7],
57 and the overall epigenetic landscape [8]. Such changes eventually trigger modifications in the
58 cardiomyocyte genetic program to increase cell contractility and favor cell survival [9]. Reactivation
59 of the fetal cardiac genetic program is a hallmark of the pathological heart, as observed in
60 pressure overload-induced hypertrophy [10].

61 Besides transforming the transcriptional landscape, post-transcriptional events, such as alternative
62 splicing (AS), RNA editing and transport, translation and degradation are also affected in cardiac
63 disease [11]. In particular, changes in AS in the pathological heart lead to alterations in the
64 expression level of numerous sarcomeric and ion channel genes associated with cardiac
65 pathologies, being determinants of cardiomyopathies and, eventually, of heart failure (HF) [12]. The
66 mechanisms presiding over RNA homeostasis permit prompt cellular adaptation to changes in the
67 external environment. This process is mainly controlled via RNA binding proteins (RBPs) that
68 physically associate with and guide RNAs through all steps of post-transcriptional control. Given
69 the importance of RBPs in RNA metabolism, their expression must be tightly controlled.

70 Among the RBPs, heterogeneous nuclear ribonucleoproteins (hnRNPs) represent a large family of
71 proteins that comprise nuclear ribonucleoprotein complexes consisting of RNA and proteins, and
72 help control mRNA dynamics [13]. Under stress conditions, hnRNPs may relocalize to a different
73 cellular compartment, undergo post-transcriptional modification, and/or exhibit altered protein
74 expression; all of these events can affect the metabolism of essential transcripts needed for cell
75 adaptation [14,15]. Indeed, the mislocalization and deregulation of hnRNPs has been associated with
76 the onset of several pathologies, including cancer, Alzheimer's disease and fronto-temporal lobe
77 dementia [16].

78 Emerging data suggest that RNA homeostasis can be controlled by mechanical cues [17–19], but the
79 molecular basis of such processes is largely unknown. One hypothesis is that mechanical stress
80 arising from the surrounding environment could affect RNA dynamics by either altering RBP
81 function or localization [20,21]. However, this process requires that components of the RNA
82 processing apparatus respond to mechanical cues generated during ECM remodeling.
83 In this study, we show ischemic and chronic cardiac pathologies are accompanied by the altered
84 expression of the RBP heterogeneous nuclear ribonucleoprotein C (hnRNPC). The protein adopts a
85 peculiar sarcomeric distribution and associates to the translation machinery upon pathological
86 ECM remodeling. Moreover, we provide evidence that hnRNPC intracellular localization can be
87 controlled by the increased biomechanical stress generated by cardiac ECM remodeling and show
88 the relocation of a fraction of the protein from the nucleus is sufficient to affect the AS of
89 transcripts coding for components of the mechanosensitive Hippo pathway. This pathway is
90 known to be heavily involved in the progression of cardiac diseases [22,23].
91 Therefore, we propose hnRNPC acts as a mechanosensitive switch affecting RNA metabolism in
92 the pathological heart.
93

RESULTS

The RNA-binding protein hnRNPC is upregulated in the diseased heart

The intense ECM remodeling occurring in cardiac pathologies can alter tissue integrity and impair organ function [5], but the underlying molecular mechanisms are unclear. We first asked whether this phenomenon was associated with a common genetic signature in both ischemic and non-ischemic heart diseases. To do so, we analyzed four published expression profiling array datasets obtained from ischemic (mouse myocardial infarction, MI) [24] and non-ischemic (mouse and human HF) [25–27] cardiac diseases and looked for common molecular function terms among the upregulated genes in the pathological heart (**Supplementary Data 1).**

We found that 11-17% of the significantly upregulated genes in MI and HF hearts (FC>1.5) shared the RNA binding (GO:0003723) annotation (**Fig. 1a; Supplementary Data 1**). When browsing the genes encoding RBPs, we found 82 RBPs that were upregulated in both mouse datasets and four that were upregulated in both human heart failure (HF) datasets. We identified hnRNPC as the only common upregulated gene among all four datasets (**Fig. 1b**). hnRNPC is a core ribonucleoprotein that is ubiquitously distributed and best known for its role as a splicing regulator [28–30]. Increased levels of this RBP have been associated with several pathological conditions [31–33]. Its upregulation in diseased cardiomyocytes has been recently confirmed by single cell RNA-sequencing in a model of ischemia-reperfusion [34].

Consistently, our *in silico* expression array analyses showed that hnRNPC was upregulated 1.52 fold 48 h after MI and 1.77 fold in HF in mice, and from 1.68 to 4.2 fold in HF patients (**Supplementary Fig. 1a**; **Supplementary Data 1**).

Given the consistent alteration in the expression level of hnRNPC in both ischemic and non-ischemic cardiac pathologies, we further analyzed its expression in heart tissue specimens obtained from a cohort of 17 patients diagnosed with end-stage HF and undergoing cardiac transplantation. As a healthy control, we used non-transplantable hearts from deceased (healthy) donors (**Supplementary Fig. 1b, c; Supplementary Table 1**). Both RT-qPCR and western blot analyses confirmed that hnRNPC gene (**Fig. 1c**) and protein (**Fig. 1d**) expression were reproducibly upregulated in failing human hearts. These results support that hnRNPC expression is upregulated in HF. This phenomenon seems to happen independently of the etiology of the pathology, since no

124 significant difference is found in ischemic vs non-ischemic heart diseases (Supplementary Fig. 1d,
125 e).

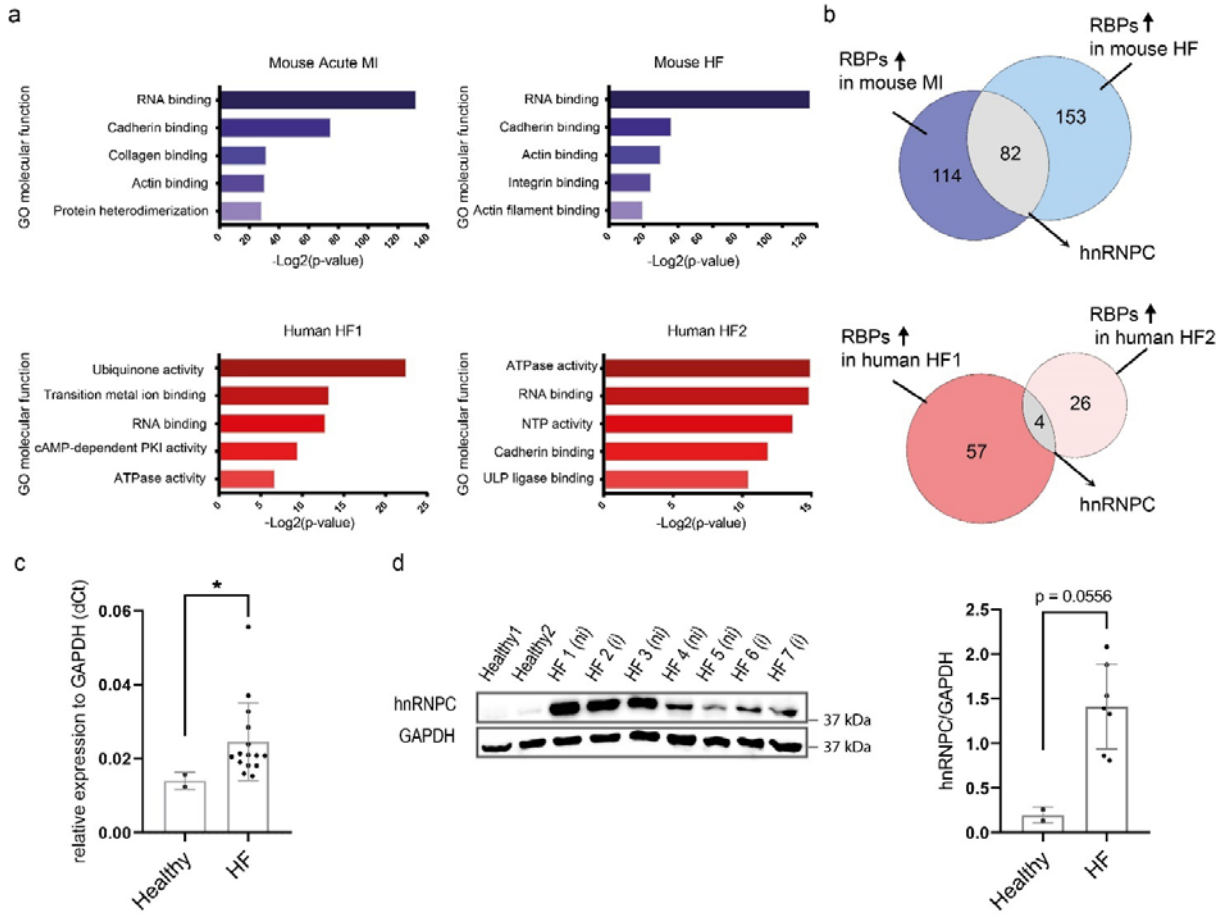

126

127 **Figure 1**: **The RNA-binding protein hnRNPC is upregulated in the diseased heart. a)** Top: Gene ontology (GO)
128 annotation of the significantly upregulated genes (FDR < 0.1; FC > 1.5) identified by expression profiling array of
129 murine hearts (left ventricle) exposed to myocardial infarction (48 h post-MI) as compared to sham operated (left) and
130 of MerCreMer (MCM) murine hearts with peak dysfunction (day 10 post-tamoxifen treatment) as compared to control
131 (right). Bottom: Gene ontology (GO) annotation of the genes found significantly upregulated by expression profiling
132 array analysis of failing (HF) human heart as compared to healthy human heart in two datasets: HF1 (left) (FDR < 0.05;
133 FC > 1.8) and HF2 (FDR < 0.1; FC > 1.5) (right). **b)** Top: Genes found upregulated by *in silico* analysis of profiling array
134 data 48 h post-MI and in HF mouse heart tissues that encode for proteins involved in RNA binding (GO: 0003723).
135 Bottom: Genes found upregulated by *in silico* analysis of profiling array data of HF1 and HF2 encoding for proteins
136 involved in RNA binding (GO: 0003723). **c)** RT-qPCR analysis of hnRNPC RNA expression in HF (N = 15; n = 2) compared
137 to healthy human hearts (N = 2; n = 2). **d)** Western blot analysis (left) and relative quantification (right) of hnRNPC
138 protein expression in samples of HF (1-7) (N = 7; n = 3) and healthy (1-2) (N = 2; n = 3) heart tissues. HF (i) and HF (ni)
139 indicate ischemic and non-ischemic samples, respectively. GAPDH was used for total protein loading normalization.
140 Data are presented as mean ± S.D.; *p < 0.05; p-values were determined by Mann-Whitney test. See also
141 **Supplementary Fig. 1** and **Supplementary Data 1**.

142

143 **hnRNPC interacts with components of the myofibril in pathological heart**

144 The participation of hnRNPs to pre-mRNA processing and mRNA dynamics is defined by their
145 cellular localization and by their interaction with specific interactors. To investigate hnRNPC
146 binding partners and how these might change upon HF, we pulled down the endogenous protein
147 in human end-stage failing and healthy heart samples and quantitatively analyzed the
148 immunoprecipitated complexes by tandem mass tag spectrometry (TMT-MS, **Fig. 2a**). We
149 identified 194 unique proteins interacting with hnRNPC in failing hearts, and 127 in healthy
150 samples: only 55 interactors were common to both conditions (**Fig. 2b; Supplementary Data 2;**
151 **Supplementary Methods**).
152
153 We weighted the specific HF and healthy interactor proteins for their abundances in the hnRNPC-
154 IP complexes and used the resulting data to build proteomaps based on the KEGG database [35]. This
155 approach allowed us to visualize how the hnRNPC interactome composition changes in the
156 pathology with a focus on the function of its binding partners (**Fig. 2c** and **Supplementary Data 2**).
157 We found that hnRNPC mainly interacted with components of the spliceosome complex in both
158 healthy and diseased hearts, consistent with its acknowledged function in RNA splicing [29,30]. More
159 interestingly, HF-specific interactors returned a common annotation for cardiac muscle
160 contraction and cytoskeletal proteins (**Fig. 2c**), suggesting that hnRNPC might display a distinct
161 localization in the pathological heart (**Supplementary Fig. 2a**).
162
163 We next performed gene ontology analysis of hnRNPC interactors in healthy and diseased heart to
164 identify which cellular component they belonged to. This analysis revealed that HF-specific
165 hnRNPC interactors included proteins belonging to the myofibril. For example, components of the
166 myofilament, sarcomere and the cardiac troponin complex were found bound to the RBP, almost
167 exclusively in HF (**Fig. 2d; Supplementary Fig. 2b**). Together with the annotation for cytosolic and
168 polysomal ribosome, which was significant for hnRNPC interactors in HF samples, these data
169 support a differential localization of the protein in the pathological heart.
170

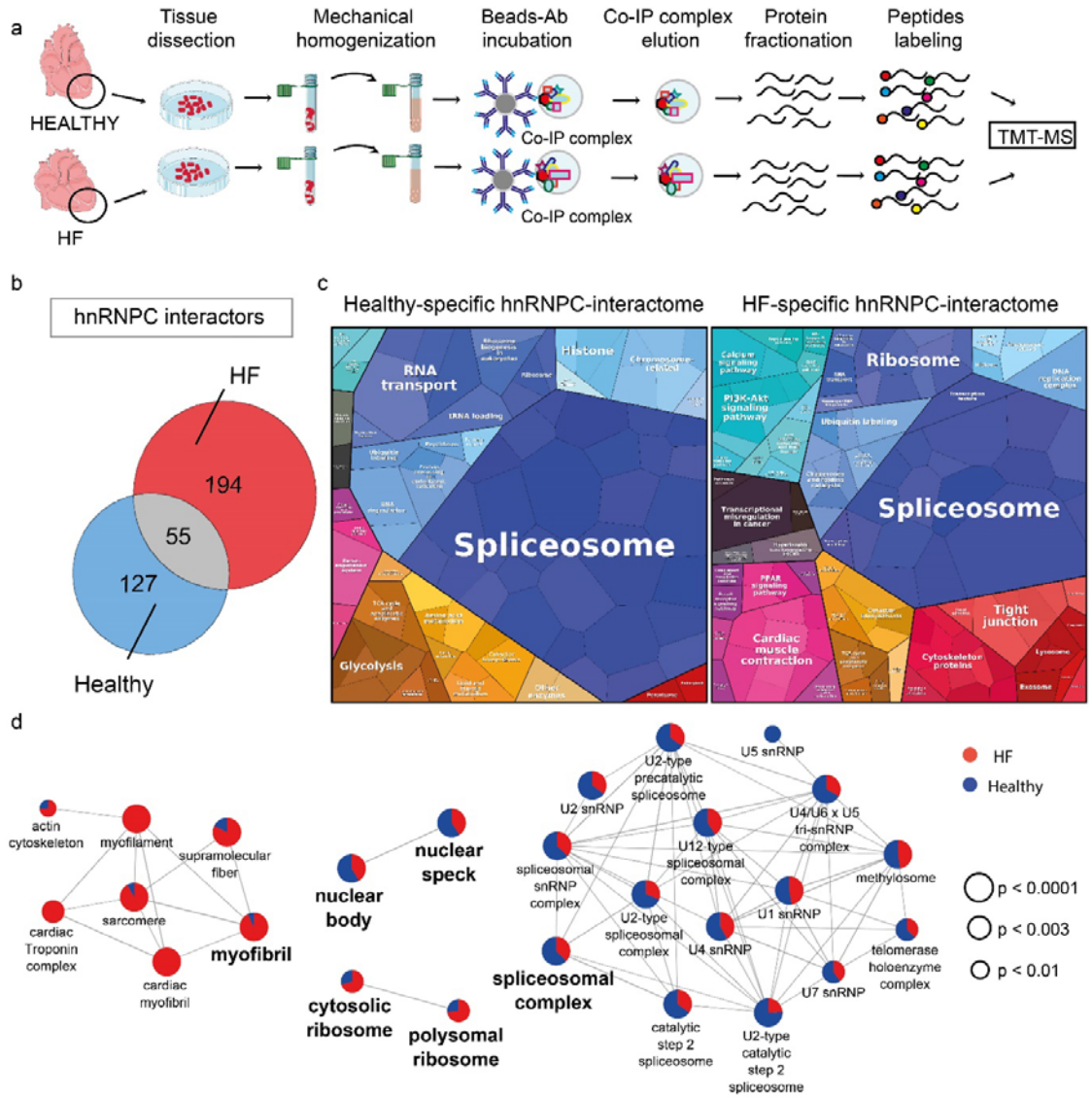

Figure 2: hnRNPC interacts with components of the myofibril in pathological heart. a) Graphical representation of the strategy adopted to identify hnRNPC interactors in the healthy human and failing heart (HF) *in vivo* by endogenous protein immunoprecipitation followed by tandem mass tag spectrometry (TMT-MS). **b)** The number of unique and shared proteins found in the hnRNPC interactome in human healthy (N=2) and HF (N=2) heart tissue by TMT-MS. **c)** Proteomaps (based on the KEGG database) representing the quantitative composition of the hnRNPC interactome in healthy and HF human hearts with a focus on protein function. Proteins are weighted for their abundance in the immunoprecipitated samples. **d)** Network representation of the cellular components Gene Ontology (GO) categories enriched in the hnRNPC interactome in healthy (red) and HF (blue) heart tissue. The size of the node indicates the Bonferroni adjusted Term p-values. See also **Supplementary Fig. 2** and **Supplementary Data 2**.

hnRNPC localizes to the Z-disk of the sarcomeric apparatus in the pathological heart

hnRNPC is predominantly localized in the nucleus. Given its interaction with components of the contractile apparatus and ribosomal proteins in the failing heart, we hypothesized hnRNPC could have a different localization under this condition. To confirm our hypothesis, we used confocal

186 microscopy to investigate hnRNPC intracellular localization in the human myocardium. Besides
187 being localized in the nucleus of cardiomyocytes, we also detected hnRNPC in the cytoplasm of the
188 contractile cells in the failing heart, with a characteristic striated pattern closely following the
189 distribution of cardiac troponin T (**Fig. 3a**). Using structured-illumination microscopy (SIM) to
190 resolve the subcellular distribution of the protein in the human pathological heart, we observed
191 that hnRNPC was localized at the Z-disc of the sarcomeres in HF (**Fig. 3b; Supplementary Fig. 3a**)
192 with a lateral resolution of ~125 nm. The shuttling of a fraction of the protein in the diseased heart
193 was confirmed by western blot analysis of nuclear and cytoplasmic extracts. This experiment also
194 indicated a significant reduction in hnRNPC nuclear expression in the pathological heart
195 (**Supplementary Fig. 3b**).
196
197 To understand whether hnRNPC sarcomeric distribution can be considered a common feature of
198 cardiac pathologies, we analyzed its localization in a mouse model of MI generated by left anterior
199 descending (LAD) coronary artery ligation in C57BL/6 mice [36] (**Supplementary Fig 3c, d)**. We
200 stained the infarction border and the distal zone of the infarcted myocardium with an antibody
201 directed against hnRNPC at day 4 post-MI, when the tissue is stormed by intense inflammatory
202 response and at day 21 post-MI, when the acute phase is resolved and the scar is stabilized [5]. As
203 expected, hnRNPC showed a characteristic nuclear localization in both the healthy and ischemic
204 heart. When co-stained with troponin T2 (TNNT2), hnRNPC displayed a clear sarcomeric pattern in
205 cardiomyocytes located at the infarct border zone 21 days post-MI. A similar pattern could be
206 detected at the earlier time-point (day 4 post-MI). Image analysis clarified the co-localization
207 between hnRNPC and TNNT2 was only significant at day 21 post-MI as compared to sham-
208 operated, day 4 post-MI. No such phenomenon was found far from the infarct, at the distal zone
209 (**Fig. 3c**). These results suggest that hnRNPC translocates to the sarcomeres in cardiomyocytes at
210 the border zone of the infarction where it interacts with components of the sarcomere. This
211 process seems to start right after the ischemic insult and consolidates during the chronic MI stage.
212 To further confirm hnRNPC sarcomeric localization in failing hearts, we performed a proximity
213 ligation assay (PLA) with TNNT2 (**Fig. 3d**; **Supplementary Data 2; Supplementary Methods**). We
214 found that hnRNPC and TNNT2 are located within 40 nm of each other in HF and that the number
215 of interactions, as indicated by PLA dots, was significantly lower in healthy hearts (**Fig. 3d**). We
216 also confirmed the physical interaction between hnRNPC and other sarcomeric proteins (FHL2,

217 PDLIM5, MYH7) identified by TMT-MS in HF but not in the healthy heart by co-
218 immunoprecipitation analysis (**Fig. 3e**).
219 In order to further corroborate hnRNPC interaction with FHL2 and PDLIM5, we pulled the two
220 endogenous proteins down in 2 HF samples and resolved the interacting proteins (**Supplementary**
221 **Data 3**). hnRNPC presence was confirmed in both IP preparations by MS analysis and by western
222 blot (**Supplementary Fig. 3e; Supplementary Data 3**). Interestingly, FHL2, PDLIM5 and hnRNPC
223 interactomes returned 143 common binding partners in the failing heart (**Supplementary Fig. 3f**)
224 with a common annotation for actin cytoskeleton and myofibril component (**Supplementary Fig.**
225 **3g**; **Supplementary Data 3**).
226 Altogether, these results indicate that hnRNPC localizes to the contractile apparatus in both
227 ischemic and non-ischemic diseased hearts. The sarcomeric distribution of hnRNPC in HF suggests
228 this protein might have distinct functions in physiological and pathological conditions.

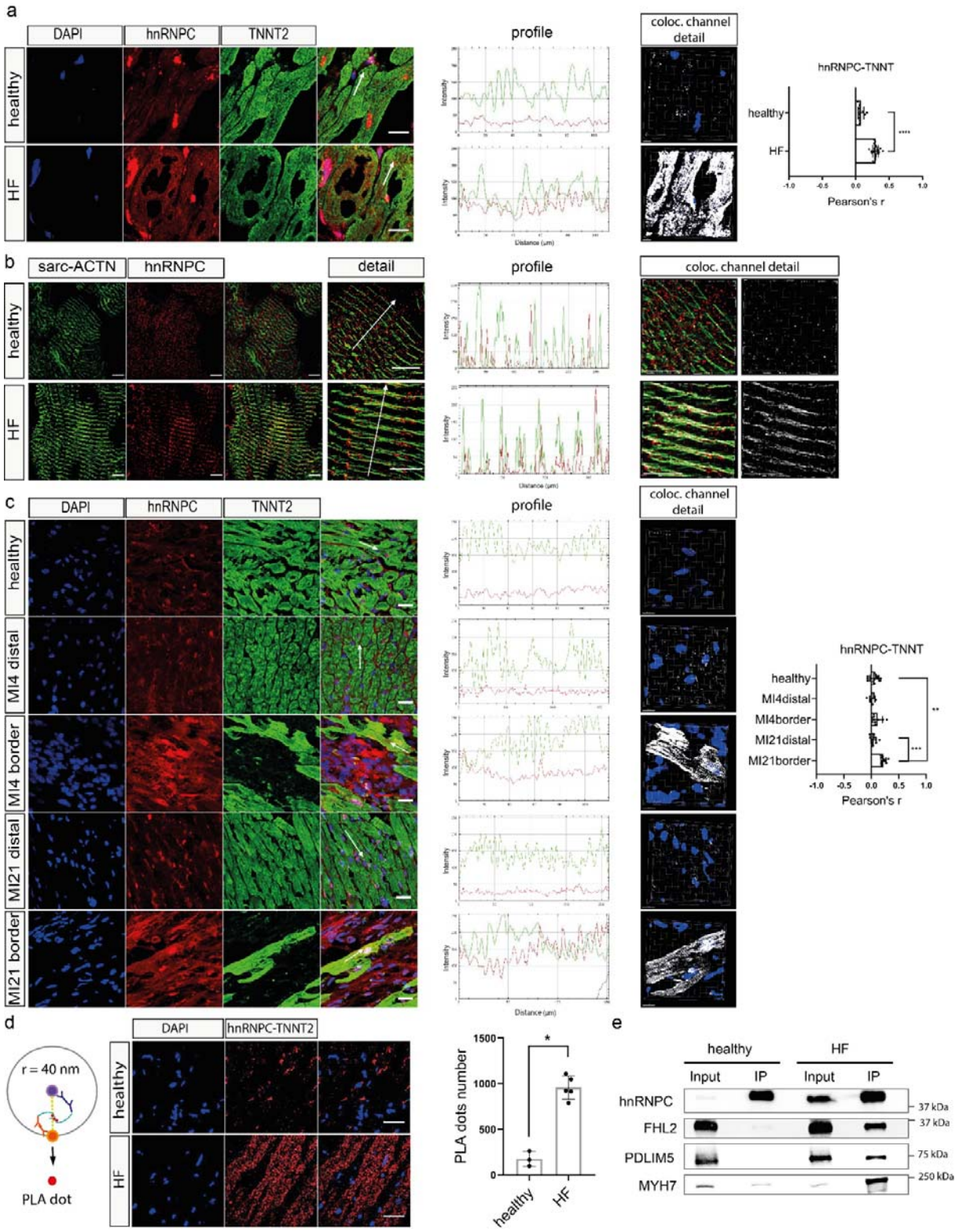

Figure 3: hnRNPC is localized at the Z-disk of the sarcomeric apparatus in the pathological heart. a) Representative confocal microscopy images depicting hnRNPC (red) localization in healthy (N=2) or failing (HF) (N=3) human heart tissue. Cardiomyocytes are stained with cardiac troponin T2 antibody (TNNT2, green) and the nuclei are

233 counterstained with DAPI (blue). The image analysis shows hnRNPC (red) distribution across the sarcomere, as
234 identified by TNNT2 staining. The area analyzed is indicated by the white arrow in the microscopic image. The detail
235 shows the colocalization (white) of red and green channels. Pearson's coefficient was calculated by Imaris ($n \geq 11$).
236 Data are presented as mean ± S.D.; ****$p < 0.0001$; Mann-Whitney test. Scale bar = 20 µm; Scale bar of detail = 5 µm.
237 **b)** Representative super-resolution image and image analysis of hnRNPC (red) sarcomeric distribution in failing HF. The
238 sarcomere is counterstained by sarcomeric alpha actinin (sarc-ACTN, green). The area analyzed is indicated by the
239 white arrow in the microscopic image. The detail shows the colocalization (white) of red and green channels. Scale bar
240 = 5 µm. **c)** Representative confocal images showing the localization and relative profile of hnRNPC (red) in healthy and
241 at the infarction proximity (border zone), or distal areas of infarcted mouse heart 4- and 21-days post-MI.
242 Cardiomyocytes are stained with cardiac troponin T (TNNT2, green) and the nuclei are counterstained with DAPI
243 (blue). The area analyzed is indicated by the white arrow in the microscopic image. The detail shows the colocalization
244 (white) of red and green channels. Pearson's coefficient was calculated by Imaris ($n \geq 8$). Data are presented as mean
245 ± S.D.; ***$p < 0.001$; **$p < 0.01$; Mann-Whitney test. Scale bar = 10 µm. **d)** Representative confocal images and
246 relative quantification of the results obtained from Proximity Ligation Assay (PLA) by using antibodies against hnRNPC
247 and TNNT2 in healthy ($N = 3$; $n \geq 12$) and HF ($N = 5$; $n \geq 13$) human heart tissue. Red dots identify areas where the
248 proteins are found to be within 40 nm of each other. The nuclei are counterstained with DAPI (blue). Data are
249 presented as mean ± S.D.; *$p < 0.05$; Mann-Whitney test. Scale bar = 50 µm. **e)** Western blot analysis of three
250 sarcomeric proteins (FHL2, PDLIM5 and MYH7) in hnRNPC immunoprecipitated samples (IP) or total lysate (input) in
251 healthy and failing human heart (HF). See also **Supplementary Fig. 3** and **Supplementary Data 3**.
252

253 **hnRNPC binds transcripts encoding components of cardiomyocytes contractile apparatus in HF**

254 To understand the role of hnRNPC at the sarcomere in HF, we next determined which transcripts it
255 physically binds. To do so, we carried out RNA-binding protein-immunoprecipitation (RIP) followed
256 by high-throughput sequencing (seq) in three human HF samples (**Fig. 4a; Supplementary**
257 **Methods**). We first confirmed the specificity of the antibody in control RIP-seq experiments in
258 which a mouse IgG antibody showed no hnRNPC immunoprecipitation (**Supplementary Fig. 4a**).
259 Next, we found that the distribution of reads on genomic regions (intron/exon, 5'UTR, 3'UTR, CDS)
260 in the hnRNPC-IP library mostly mapped to intronic regions (63%), followed by coding DNA
261 sequences (CDS, 22%), 3' (13%) and 5' (2%) untranslated regions (UTRs) (**Fig. 4b**). After browsing
262 the POSTAR2 database, we confirmed that 2,487 out of 2,629 RNA targets found in our RIP-seq
263 experiment harbored at least one binding site for hnRNPC [37] (**Supplementary Fig. 4b**).
264

265 Next, we calculated the number of reads mapping to a specific region (intron/exon, 5'UTR, 3'UTR,
266 CDS) for each gene. By this approach, we could define two groups of targets: the transcripts
267 enriched in intronic and those enriched in exonic reads (exon, CDS, 5' and 3' UTRs)
268 (**Supplementary Fig. 4c; Supplementary Data 4; Supplementary Methods**). The large proportion
269 of intronic hits is consistent with the documented role of hnRNPC in pre-mRNA splicing [28].
270 Although RBPs can regulate pre-mRNA splicing by binding to exonic splicing enhancers or silencers

271 [38], we hypothesized that the exon-enriched targets found in the pathological heart could represent
272 mature RNAs that might be informative as to hnRNPC activity at the sarcomere.
273 We then performed gene ontology analysis of hnRNPC-targets to understand to which cellular
274 component they belonged to. Here, we identified that the intron-enriched targets (1,681) mostly
275 belonged to nucleus, cytoskeleton and adhesion categories, while 18.8% of all annotated I-band
276 components were hnRNPC targets (**Fig. 4c, Fig. 4d**). Among the intron-enriched targets belonging
277 to the I-band category, we found transcripts such as LDB3, CACNA1C, DMD, PDLIM5, for which an
278 alteration in AS has been previously assigned to the occurrence of cardiac pathologies [12,39].
279 Moreover, we found splicing regulators among the hnRNPC targets (including RBM20, MBNL2,
280 CELF1-2, RBFOX1-2) that are involved in heart development and disease [40,41]. These findings
281 indicate that hnRNPC could exert both a direct and indirect role in splicing control of sarcomeric
282 transcripts affecting the post-transcriptional regulation of other RBPs. Selected hnRNPC intron-
283 enriched targets, showing high read coverage on intronic regions, as obtained by Integrative
284 Genomics Viewer (IGV), are shown in **Fig. 4e** and in **Supplementary Fig. 4d.**
285
286 We performed a similar cellular component enrichment analysis of the hnRNPC exon-enriched
287 targets and identified a significant enrichment for the myofibril, troponin complex, A and I bands
288 of the sarcomeres (**Fig. 4f**). Titin (*TTN*), cardiac muscle alpha actin (*ACTC1*) and troponin I (*TNNI3*)
289 contractile apparatus transcripts were found among hnRNPC targets (**Fig. 4g; Supplementary Fig.
290 4e**). When we analyzed the enriched biological processes by these exon-enriched hnRNPC targets,
291 we found that these targets were mainly involved in muscle structure development (22), filament
292 sliding (9), contraction (14) and myofibril assembly (9) (**Supplementary Fig. 4f**). By comparison, the
293 intron-enriched targets were principally associated with the regulation of signal transduction
294 (472), cell communication (513), cytoskeletal organization (209) and heart development (113)
295 (**Supplementary Fig. 4g**).
296
297 These data demonstrate that hnRNPC interacts with intron-enriched transcripts, confirming its
298 well-known function as a splicing regulator. On the other hand, hnRNPC also binds exon-enriched
299 transcripts that are enriched in RNAs encoding myofibril components. This finding suggests a
300 possible implication of hnRNPC in translational regulation of selected targets upon its
301 relocalization to the sarcomeres in HF.

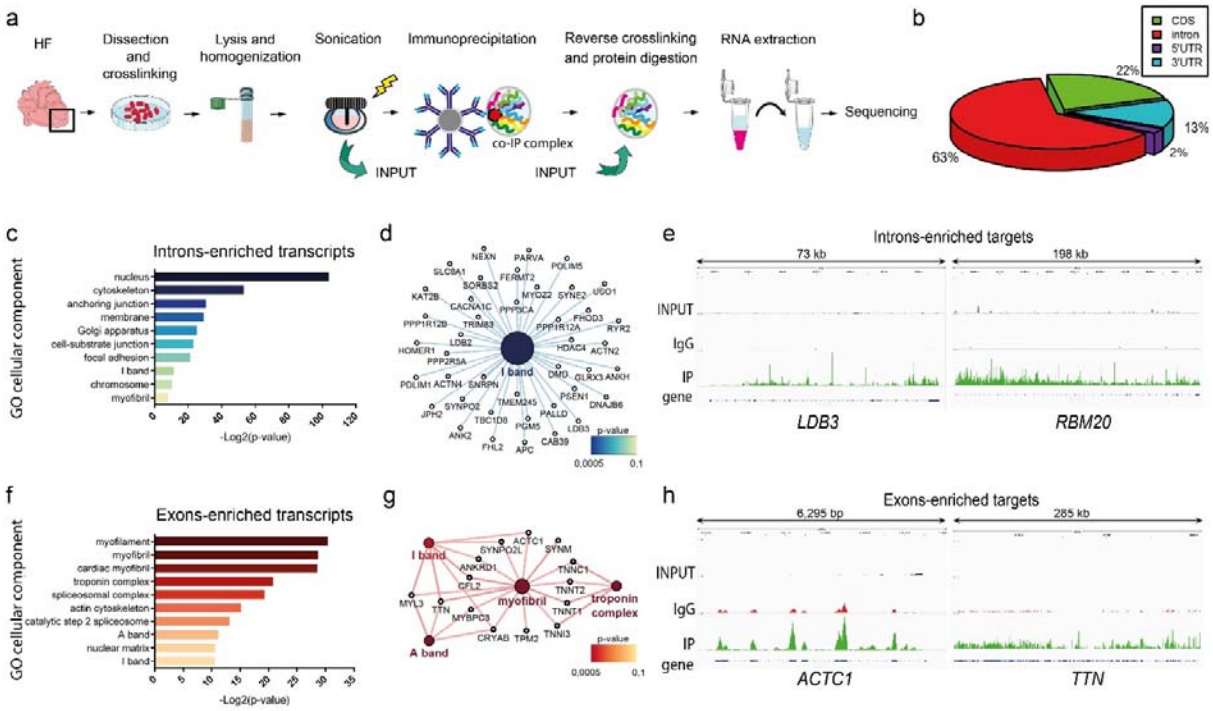

Figure 4: hnRNPC binds transcripts encoding components of cardiomyocytes contractile apparatus in HF. **a)** Graphical representation of the strategy adopted to identify hnRNPC RNA targets in human heart failure (N = 3) (HF) *in vivo* by endogenous RNA immunoprecipitation followed by sequencing. **b)** Genomic distribution of the read counts showing the percentage of reads mapping on specific genomic regions (intron/exon, 5'UTR, 3'UTR, CDS) in immunoprecipitated samples (N = 3). **c)** Cellular components Gene Ontology (GO) categories significantly enriched in intron-enriched transcripts (log2 intron/exon ratio > 1) bound to hnRNPC in HF. **d)** GO network of I band cellular components and the intron-enriched transcripts within this network that bind hnRNPC (p-value corrected with Bonferroni = 0.00037). The size of the node is proportional to the number of hnRNPC targets belonging to the ontology. **e)** Individual gene representation of intron-enriched hnRNPC targets: read coverage is displayed in INPUT (black), IgG (red) and IP (green) samples. **f)** Cellular components GO categories significantly (p-value < 0,05) enriched in exon-enriched transcripts (log2 intron/exon ratio < -1) bound to hnRNPC in HF. **g)** GO network of cellular components of interest enriched (Group p-value corrected with Bonferroni = 9.43E-07) in exon-enriched RNAs that bind hnRNPC in HF. The size of the node is proportional to the number of hnRNPC targets belonging to the ontology. **h)** Individual gene representation of exon-enriched hnRNPC targets: read coverage is displayed in INPUT (black), IgG (red) and IP (green) samples. See also **Supplementary Fig. 4** and **Supplementary Data 4**.

ECM pathological remodeling induces hnRNPC association to the translation machinery at the sarcomere

Because hnRNPC exon-enriched targets comprised mainly mRNAs encoding sarcomeric proteins and we found hnRNPC localized at the sarcomere in HF, we queried the role of hnRNPC at this site. *TTN*, *ACTC1* and *TNNI3* transcripts, found among hnRNPC exon-enriched targets, are translated at the sarcomeres in the rat heart, in a process dubbed as 'localized translation' [42,43]. Localized translation allows for the spatio-temporal control of contractile protein synthesis at the

326 sarcomeric site [43,44]. Previous reports have shown ribosomes are present at the sarcomeres in the
327 rat heart, where localized translation ensures that contractile proteins are readily replaced during
328 sarcomere remodeling [43,45]. Consistently, our TMT-MS analysis identified nine ribosomal proteins
329 in the hnRNPC interactome in the failing heart (**Supplementary Fig. 5a**) which accounted for the
330 ribosome annotation found in GO cellular component analysis (**Fig. 2d**). To confirm the presence
331 of the ribosomes at the sarcomeric structure, we labeled the evolutionarily conserved RPS6
332 ribosomal protein (which was a potential hnRNPC interactor in our TMT-MS analysis) in healthy
333 and HF cardiac tissue sections. We found a typical sarcomeric cross-striated pattern, as confirmed
334 by TNNT2 decoration, in both groups (**Supplementary Fig. 5b**). We observed a similar pattern in
335 the sarcomeres of cardiomyocytes residing both at the distal and at border zones of myocardial
336 infarction, as well as in healthy cardiomyocytes in the murine heart (**Supplementary Fig. 5c**).
337
338 As we found that hnRNPC relocated to the sarcomeres in HF and confirmed the presence of the
339 ribosomes at this site in the human heart, we asked whether sarcomeres could be a site of
340 localized translation in human cardiomyocytes. Therefore, we derived contractile cardiomyocytes
341 from human induced pluripotent stem cells (iPSC-CMs) through an established protocol [46]. In
342 differentiated cells, we first confirmed RPS6 presence at the sarcomeres by co-localization analysis
343 of the protein with cardiac TNNT2 (**Fig. 5a**). Next, we performed a ribopuromycylation assay that
344 exploits puromycin mimicry of aminoacylated tRNA to visualize the active sites of translation
345 (**Supplementary Fig. 5d**). Here, puromycin (PMY) could be incorporated in the contractile
346 apparatus of human iPSC-CMs, thus demonstrating human cardiomyocyte sarcomeres are active
347 sites of protein translation (**Fig. 5b**).
348
349 Next, we queried whether hnRNPC associates to the translation machinery when localized at the
350 sarcomeres in the pathological heart. To do this, we adopted an original reductionist approach
351 that proved effective at reproducing some key mechanical features of pathological cardiac ECM
352 remodeling by decellularizing healthy and diseased human heart tissue (dECMs) [23,47]. We used the
353 homogenized dECMs to coat the surface of cell culture plates. Next, we seeded contractile iPSC-
354 CMs on healthy and pathological dECMs and combined ribopuromycilation with PLA assay to
355 investigate whether hnRNPC localized close to the active translation sites, as indicated by PMY
356 staining (**Fig. 5c**). The analysis showed the presence of PLA dots, corresponding to hnRNPC–PMY

proximity, in TNNT2-positive cells cultured on pathological dECMs but not in iPSC-CMs grown on healthy dECMs (**Fig. 5d**). These data confirm that sarcomeres are active sites of RNA translation and that hnRNPC localizes to those sites as a result of cardiac ECM pathological remodeling.

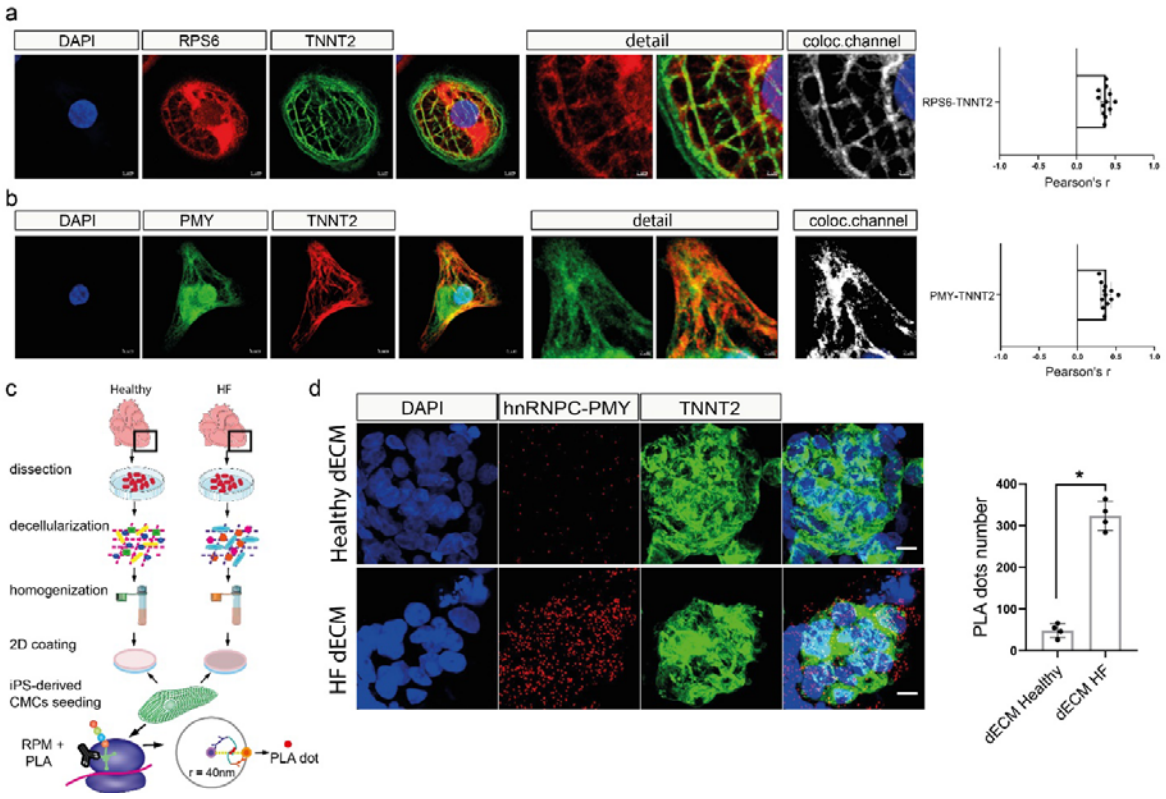

Figure 5: hnRNPC associates to the translation machinery at the sarcomere following ECM pathological remodeling. a) Representative confocal image of ribosomal protein S6 (RPS6, red) localization in iPSC-derived contractile cardiomyocytes (N = 3). Sarcomeric units are identified by cardiac troponin T (TNNT2, green) staining and nuclei are counterstained with DAPI (blue). The detail shows a magnified area of a single cardiomyocyte in which the colocalization of red and green channels has been quantified using Imaris software (n = 12). Data are presented as mean ± S.D. Scale bar = 5 µm; Scale bar of detail = 2 µm. **b)** Representative confocal microscopy images of single iPSC-derived cardiomyocytes labeled with anti-puromycin antibody (PMY, green) after puromycin incorporation (N = 3). Sarcomeric units are identified by cardiac troponin T (TNNT2, red) staining and the nuclei are counterstained with DAPI (blue). Colocalization analysis of the green and red channels was quantified by Imaris software (n = 12). Data are presented as mean ± S.D. The detail shows a magnified area of a single cardiomyocyte. Scale bar = 5 µm; Scale bar of detail: 2 µm. **c)** Description of the ribopuromycilation and Proximity Ligation Assay (PLA) used to investigate the occurrence of localized translation at the sarcomeres in iPSC-derived cardiomyocytes grown onto decellularized matrices obtained from either healthy or failing human hearts. **d)** Representative confocal microscopy images of PLA using antibodies against PMY and hnRNPC in iPSC-derived beating cardiomyocytes grown onto HF or healthy decellularized heart matrices. The cardiomyocytes were labeled with cardiac troponin T (TNNT2, green). Red dots indicate that the proteins are within 40 nm of each other. The nuclei are counterstained with DAPI (blue). Data are presented as mean ± S.D. (N = 4; n = 6). *p < 0.05; Mann-Whitney test. Scale bar = 10 µm. See also **Supplementary Fig.5**.

hnRNPC intracellular localization is controlled by cell spreading and cytoskeletal tension

382 Thus far we have shown that cardiac ECM pathological remodeling induces hnRNPC shuttling to
383 the active sites of translation at the sarcomere. Pathological remodeling is a complex
384 phenomenon modifying the chemical composition and the mechanical properties of cardiac ECM
385 [5,23]. We tried to disentangle the role of mechanical cues in hnRNPC localization. We hence adopted
386 surfaces with the same chemical composition and controlled rigidities (1.5 vs 28 kPa) and repeated
387 the ribopuromycilation assay followed by PLA on iPSC-CMs. The elasticity values chosen do not
388 exactly match those found in the living heart, but are in the same kPa range. More importantly,
389 these values have been shown to induce mechanosensor activation in other cell systems [48–50].
390 Here we found hnRNPC localization to the sites of active translation, as detected by PMY
391 interaction, was sensitive to the stiffness of the substrate, since PLA signal was significantly
392 different on substrates with different elasticities. This result suggests that substrate stiffness *per*
393 *se* can induce hnRNPC shuttling (**Supplementary Fig. 6a**).

394 In order to corroborate this result, we challenged normal human dermal fibroblasts (NHDFs), a
395 model of highly mechano-responsive cells, with different mechanical stimuli and analyzed hnRNPC
396 distribution. Here, we used a fibrin-based 3D culture system, whose mechanical properties can be
397 tuned in a physiological range by modulating the fibrinogen concentration in the presence of
398 constant levels of thrombin [51] (**Supplementary Fig. 6b**). We embedded NHDFs into the hydrogels
399 and analyzed hnRNPC localization after 48 hours. We additionally stained F-actin and cell nuclei to
400 monitor cell ability to spread within the hydrogels, indicative of the degree of cytoskeletal tension.
401 We observed that NHDFs spread well in soft (2 mg/ml and 5 mg/ml fibrinogen) hydrogels, but
402 failed to elongate as the stiffness of the fibrin gel increased (17 mg/ml fibrinogen). At the highest
403 fibrinogen concentration (50 mg/ml), the cells were unable to acquire an elongated morphology
404 (**Supplementary Fig. 6c**). Image analysis demonstrated that hnRNPC nuclear localization correlated
405 with the NHDF volume and with the cellular ability to spread within soft hydrogels, with hnRNPC
406 translocation to the cytoplasm characteristic of cells confined into stiff fibrin gels (**Fig. 6a;**
407 **Supplementary Fig. 6c**). These data suggest that hnRNPC nuclear localization might be controlled
408 by the ability of cells to develop intracellular tension and spread within the surrounding milieu.

409 To corroborate our hypothesis, we used fibronectin-coated micro-patterned surfaces to precisely
410 control single cell area [49,50,52]. We stained NHDFs with a specific antibody against hnRNPC and
411 used YAP as an example of a mechanosensitive protein whose localization depends on intracellular

412 tension and cell spreading [49,50]. Confocal analysis showed that hnRNPC localized at the nucleus in
413 cells that were confined to bigger areas (2,025 μm^2) or free to spread. By contrast, the protein
414 shuttled to the perinuclear region of cells constrained on smaller surfaces (1,024 and 300 μm^2)
415 (**Fig. 6b; Supplementary Fig. 6d**). To resolve the intracellular distribution of the protein, we
416 counterstained the nuclear structure with Lamin A/C and visualized the cells by structured
417 illumination microscopy (SIM). Here we found that hnRNPC egressed the nucleus and acquired a
418 perinuclear localization in constrained cells, with a peculiar distribution close to Lamin A/C nuclear
419 invaginations (**Fig. 6c**). We repeated the same experiment using iPSC-CMs and again observed that
420 hnRNPC nuclear localization was also sensitive to cell spreading in contractile cells
421 (**Supplementary Fig. 6e**).
422 Having shown that hnRNPC nuclear localization required the cell to spread in 2D and 3D, we next
423 performed in depth experiments to clarify whether the shuttling of the protein was driven by the
424 availability of adhesion sites within the local ECM or by the transmission of intracellular tension.
425 We first designed single cell fibronectin-coated micropatterned arrays that keep the cell area
426 constant (4,900 μm^2), while reducing the number of fibronectin adhesion spots [49]. When we
427 decreased the adhesion area (1,000 and 450 μm^2), we saw no significant effect on hnRNPC
428 nuclear localization (**Fig. 6d**).
429
430 We concluded that adhesion did not affect hnRNPC localization, and decided to inhibit the
431 transmission of intracellular tension by treating NHDFs with pharmacological inhibitors of either
432 the RhoA/ROCK pathway (Y27632) or F-actin polymerization (Latrunculin A) [2,53]. We analyzed
433 hnRNPC localization in the nucleus and cytoplasm by cell fractionation followed by western
434 blotting, and detected a significant decrease in nuclear hnRNPC and the concomitant increase in
435 its cytoplasmic expression in cells treated with the pharmacological inhibitors (**Fig. 6e**). These data
436 are consistent with the hypothesis that the inhibition of intracellular tension determines a
437 reduction in hnRNPC nuclear expression and the shuttling of a fraction of the protein to the
438 cytoplasm.

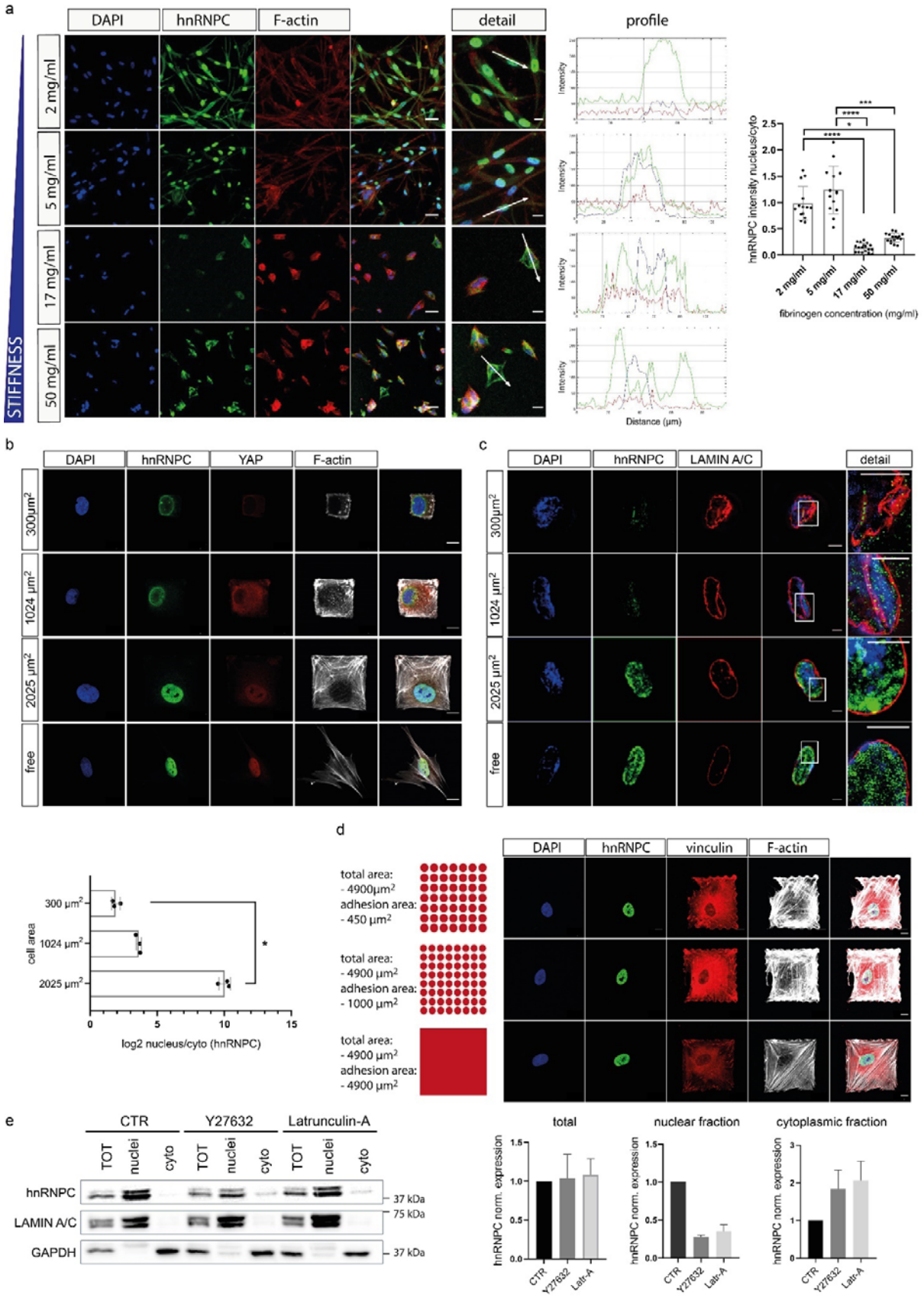
a
DAPI
hnRNPC
F-actin
detail
profile
STIFFNESS
2 mg/ml
5 mg/ml
17 mg/ml
50 mg/ml
Intensity
Distance (µm)
hnRNPC intensity nucleus/cyto
fibrinogen concentration (mg/ml)
b
DAPI
hnRNPC
YAP
F-actin
300µm²
1024 µm²
2025 µm²
free
c
DAPI
hnRNPC
LAMIN A/C
detail
cell area
log2 nucleus/cyto (hnRNPC)
d
total area:
- 4900µm²
adhesion area:
- 450 µm²
total area:
- 4900 µm²
adhesion area:
- 1000 µm²
total area:
- 4900 µm²
adhesion area:
- 4900 µm²
DAPI
hnRNPC
vinculin
F-actin
e
CTR
Y27632
Latrunculin-A
TOT
nuclei
cyto
hnRNPC
LAMIN A/C
GAPDH
37 kDa
75 kDa
total
nuclear fraction
cytoplasmic fraction
hnRNPC norm. expression
CTR
Y27632
Latr-A

439

440 **Figure 6: hnRNPC intracellular localization is mechanically controlled. a)** Left: Representative confocal
441 microscopy images showing hnRNPC (green) expression in normal human dermal fibroblasts (NHDFs) embedded for
442 48 h in fibrin-based hydrogels with an increasing fibrinogen concentration and stiffness. Cellular F-actin was labeled
443 with Phalloidin (red) and the nuclei were counterstained with DAPI (blue). Image analysis shows the quantification of
444 signal distribution in NHDFs embedded for 48 h in fibrin-based hydrogels with controlled stiffness. Right:
445 Quantification of the hnRNPC in the nucleus/cytoplasm distribution in fibrin-gels with increasing fibrinogen
446 concentration and stiffness. For each experimental condition, data are presented as mean ± S.D. from N ≥ 7
447 independent fields of acquisition; *p < 0.05; ***p < 0.001; ****p < 0.0001, Kruskal-Wallis test followed by Dunn's
448 multiple comparison test. **b)** Top: confocal analysis of individual cells grown onto 300, 1024, 2025 μm^2 micropatterns
449 coated with fibronectin. The cells were labeled with anti-hnRNPC (green), Alexa Fluor 647 Phalloidin, anti-Lamin A/C
450 (red) and the nuclei were counterstained with DAPI (blue). Bottom: Barplot representation of hnRNPC
451 nucleus/cytoplasm distribution in single cells seeded onto 300, 1024, 2025 μm^2 micropatterns (N = 3; n ≥ 8); *p < 0.05;
452 Kruskal-Wallis test followed by Dunn's multiple comparison test. **c)** Representative super-resolution images of
453 individual cells grown onto 300, 1024, 2025 μm^2 micropatterns coated with fibronectin. The cells were labeled with
454 anti-hnRNPC (green) and anti-Lamin A/C (red). Nuclei were counterstained with DAPI. **d)** Left: Annotation of
455 micropattern properties (cell area and adhesion area) and a schematic top view of the fibronectin distribution in the
456 micropatterns. Red color indicates fibronectin-covered area. Right: Confocal images of single NHDFs grown onto the
457 indicated micropatterns and labeled with anti-vinculin (red), anti-hnRNPC (green), Alexa Fluor 546 Phalloidin and DAPI
458 (blue) (N = 3; n = 5). **e)** Western blot analysis (left) and quantification (right) of hnRNPC expression in cellular (TOT),
459 nuclear and cytoplasmic fractions of NHDFs treated or not (CTR) with Latrunculin-A and Y27632 inhibitors. GAPDH was
460 used for loading normalization of the total and cytoplasmic fractions. Lamin A/C was used to normalize protein loading
461 in the nuclear fraction. Band intensities corresponding to hnRNPC in the nuclear and cytoplasmic fractions were
462 quantified using Bio-Rad Image Lab software. Data are presented as mean ± S.D. (N = 3). See also **Supplementary Fig.**
463 **6**.
464

465 **hnRNPC regulates the AS of genes involved in mechanotransduction**

466 We have so far demonstrated that a fraction of hnRNPC is distributed to the sarcomeres in HF, and
467 its expression in the nucleus is reduced (**Supplementary Fig. 3b**). This data suggests a decreased
468 contribution of the ribonucleoprotein to the splicing process (**Fig. 2c)**. Moreover, we found that
469 altered cytoskeletal tension affects hnRNPC subcellular localization. As hnRNPC is associated to
470 the spliceosome and mainly nuclear in physiological conditions, we studied which changes in
471 terms of AS events would cause the reduced contribution of hnRNPC to the splicing process. We
472 therefore knocked down (KD) hnRNPC in NHDFs using two independent siRNAs (**Fig. 7a**) and
473 analyzed the abundance of RNA splicing variants by high throughput genome-wide RNA-seq. We
474 then adopted the multivariate analysis of transcript splicing (MATs) statistical algorithm to
475 quantify the changes in AS driven by hnRNPC downregulation. We identified the differential
476 splicing of 2,032 RNA transcripts (FDR< 0.01 and |ΔPSI| ≥ 0.1) in KD cells, as compared to the
477 scrambled control transfected cells (**Supplementary Data 5; Supplementary Methods**). Consistent
478 with previous reports [30,54], most of the splicing events affected by hnRNPC KD consisted of skipped

479 exons (SE: 78,95%), followed by mutually exclusive exons (MXE: 14,85%), alternative 3'-5' splice
480 sites (A3SS: 3,76% and A5SS: 2,15%) and intron retention (IR: 0,3%) (**Fig. 7b**). Pathway enrichment
481 analysis of the 2,032 differentially spliced genes in hnRNPC KD cells revealed that the splicing of
482 numerous genes involved in cell mechanotransduction, integrin-mediated cell adhesion and focal
483 adhesion was affected (**Fig. 7c**). In particular, 15 components of the Hippo signaling pathway, a
484 mechanosensitive molecular axis involved in heart development [22] and diseases [52,55], displayed
485 altered AS upon hnRNPC silencing (**Supplementary Data 6**).
486 Among the 15 genes belonging to Hippo pathway which displayed altered splicing upon hnRNPC
487 depletion we found the main effector, Yes Associated Protein 1 (YAP1). *YAP1* gene encodes for
488 multiple protein isoforms (**Fig. 7d**). The distinct co-transcriptional fingerprints of the splicing
489 variants are known to depend upon the presence of one (YAP1-1) or two (YAP1-2) WW domains
490 [56,56]. The exon 4, which encodes for the second WW domain in YAP1-2 isoforms, was found
491 differentially spliced in hnRNPC-depleted cells by RNA-seq. We thus analysed the inclusion of exon
492 4 in YAP1 transcript upon hnRNPC KD by calculating the relative abundance of YAP1 isoforms
493 including (YAP1-2) or not (YAP1-1) exon 4 by RT-qPCR and by conventional PCR. Interestingly, we
494 found that hnRNPC depletion promotes the inclusion of exon 4 in YAP1 transcript and affects the
495 overall balance among YAP1-1 and YAP1-2 splicing variants (**Fig. 7d, e Supplementary Fig. 7a**).
496 These results were confirmed in hnRNPC-depleted iPSC-CMs (**Supplementary Fig. 7b, c**).
497 Additionally, we obtained similar results by treating NHDF with inhibitors of cytoskeletal tension
498 (**Fig. 7e**). Hence we established that the mechanical displacement of hnRNPC from the nucleus
499 affects the splicing of YAP1 by promoting exon 4 inclusion (**Fig. 7e**).

500 In order to validate this set of data, we analyzed the expression of the variable exon 7 of CD44
501 transcript, whose alternative splicing has been proven mechanosensitive [57]. As expected, here we
502 found the inclusion of variable exon 7 in CD44 transcript increases upon hnRNPC depletion as well
503 as upon treatment with inhibitors of tension in NHDFs (**Supplementary Fig. 7d**). We could only
504 confirm this result in one out of the two iPSC-CMs depleted for hnRNPC (**Supplementary Fig. 7e)**.
505 This discrepancy could be explained by the variability in differentiation efficiency in distinct iPSC
506 cultures or by the use of two unrelated siRNAs in the KD experiments.
507 We also validated the reduced expression of MYLK exon 11 and COL6A3 exon 3 found by RNA-seq
508 in hnRNPC KD cells by RT-qPCR (**Supplementary Fig. 7f, g**).

509 Next, we compared the differentially spliced genes in hnRNPC KD cells to the RNAs known to
510 harbor hnRNPC binding sites (as documented in the POSTAR database). We found as many as
511 1,738 among the 2,032 transcripts had at least one hnRNPC binding site and could, in principle,
512 interact with this RBP (**Supplementary Fig. 7h**). In order to check that those were true hnRNPC
513 targets, we performed individual-nucleotide resolution Cross-Linking and ImmunoPrecipitation
514 (iCLIP). This approach allowed us to map precisely hnRNPC-RNA interactions and relate them to
515 the previously detected hnRNPC-dependent splicing events in NHDF cells (**Supplementary Fig. 8a,**
516 **b; Supplementary Data 7; Supplementary Methods**). A total of 1,470,396 uniquely mapped
517 hnRNPC crosslink events were identified, which cluster into 13,567 binding sites in 5,536
518 transcripts (**Supplementary Data 7**). As a control, we found the majority of hnRNPC crosslink
519 events to be located within introns, with high coverage of Alu elements, in good agreement with
520 previous results obtained in other cell types [28,29] (**Supplementary Fig. 8c, d**). While 58% of the
521 crosslink events mapped to coding sequences, several non-coding hnRNPC targets were also
522 identified, including MALAT-1, a long non coding RNA whose interaction with hnRNPC has already
523 been described [58] (**Supplementary Fig. 8e-g**).
524 Next, we matched the results of AS events in hnRNPC KD cells with those obtained by iCLIP. In
525 particular, we searched for all transcripts directly bound by hnRNPC to determine whether they
526 displayed AS in hnRNPC-depleted cells. We ultimately detected 748 transcripts physically
527 interacting with hnRNPC in NHDFs that were differentially spliced in the absence of the protein
528 (**Fig. 7f; Supplementary Data 7**). Among those, we confirmed the presence of seven components
529 of the Hippo pathway (**Fig. 7g; Supplementary Data 6**), on which hnRNPC binding occurred in
530 intronic regions surrounding exons alternatively spliced in hnRNPC-depleted cells (**Fig. 7h, i;**
531 **Supplementary Fig. 9a, b).** This was the case for YAP1 transcript, for which, the RNA-binding
532 protein iCLIP coverage in the proximity of the hnRNPC-dependent exon 4 could be confirmed (**Fig.**
533 **7h, i**). The data were validated by independent iCLIP-PCR assay for three selected hnRNPC targets:
534 YAP1, CD44 and MYLK (**Supplementary Fig. 10 a, b**). In summary, these results suggest that
535 hnRNPC is directly involved in the regulation of AS of pre-mRNAs encoding genes involved in
536 mechanotransduction.

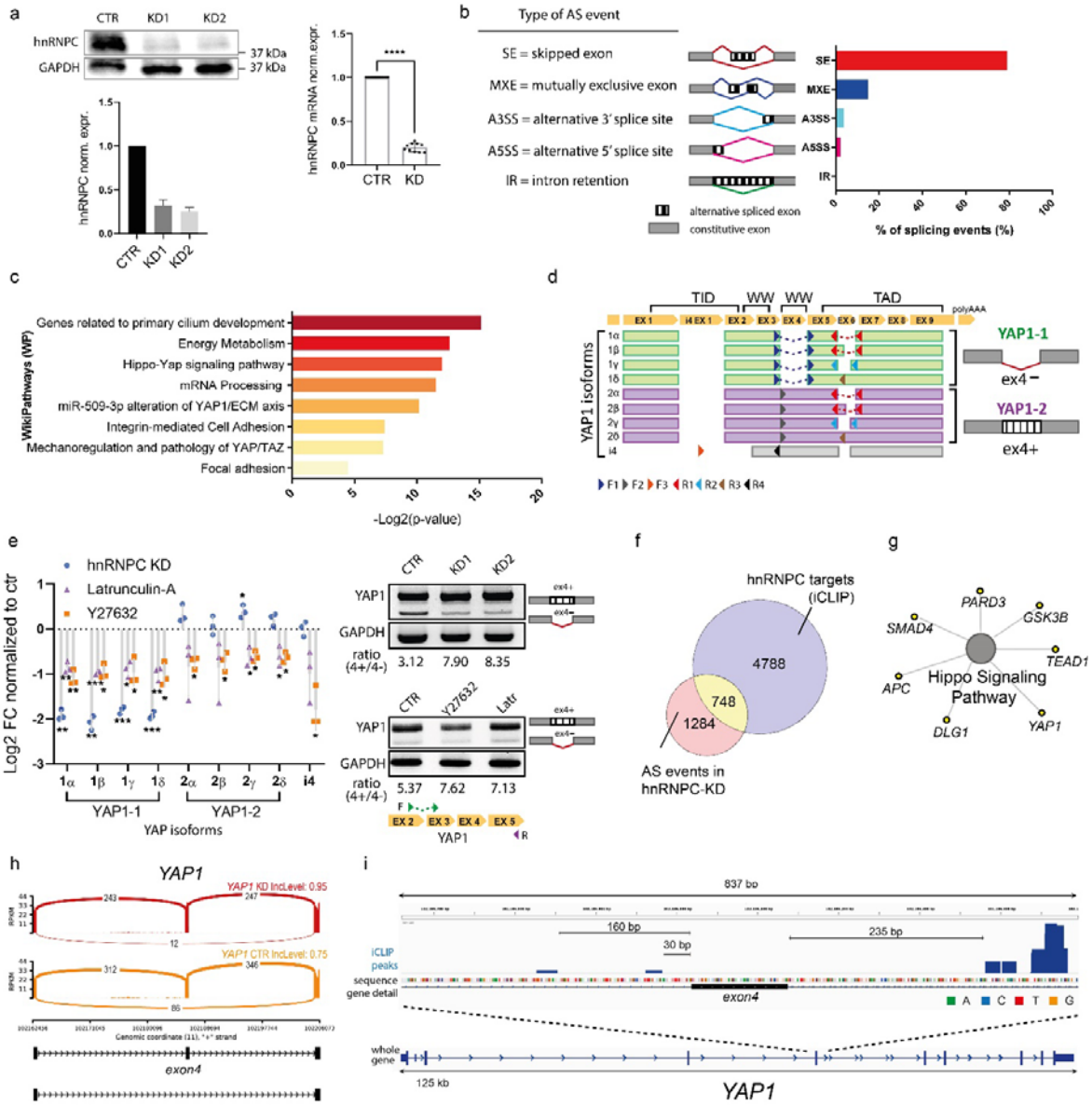

Figure 7: hnRNPC regulates the alternative splicing of genes involved in mechanotransduction. a) Left: Western blot analysis (top) and relative quantification (bottom) of hnRNPC protein expression in normal human dermal fibroblasts (NHDF) transfected with hnRNPC siRNA constructs (KD1 and KD2) or with a control siRNA construct (CTR). Protein expression was assessed 96 h after the transfection. GAPDH was used for total protein loading normalization. Data are presented as mean ± S.D. (N = 3). Right: histogram representation of the results obtained by RT-qPCR analysis of hnRNPC RNA expression in NHDFs 96 h after transfection with hnRNPC (KD) or control siRNAs (CTR). Data are presented as mean ± S.D. (N = 10). ****p < 0.0001, Mann-Whitney test**. b)** The percentage of splicing events occurring in hnRNPC KD cells classified into the five major categories of alternative splicing (AS), as obtained by Multivariate analysis of transcript splicing (MATs). **c)** Gene ontology (GO) analysis showing the main pathways found significantly enriched (p-value < 0.05) in genes displaying altered splicing in hnRNPC KD cells using the WikiPathways database. **d)** Schematic representation of protein-coding YAP1 isoforms. Left) Coding regions (CDS) of four YAP1-1, four YAP1-2, and YAP-i4 isoforms are aligned and corresponding protein domains (TEAD-binding domain (TBD), WW domains, TRANS-activating-domain (TID) with N-terminal coiled-coil domain and N terminal PDZ motif) are shown. The arrows represent the approximate binding sites of forward (F) and reverse (R) primers used to detect the specific isoforms. Right) schematic representation of the AS event (exon 4 skipping) that distinguishes YAP1-1 from YAP1-2

553 isoforms. **e)** Left) Dotplot representation of YAP isoforms mRNA expression (Log2FC) in NHDF upon hnRNPC-depletion
554 (blue) or upon 24h treatment with latrunculin-A (purple) or rock inhibitor (Y27632) (orange). Each result is compared
555 to its relative control. Superimposed bars represent the as mean ± S.D. (N = 3). *p < 0.05; **p < 0.01; ***p < 0.001;
556 One-sample t-test. Right) RT-PCR of YAP1 in NHDF upon hnRNPC depletion (Top) or upon 24h treatment with
557 inhibitors of tension (Latrunculin (Latr) and Y27632) (Bottom). Top band: exon 4-included YAP1 mRNA. Bottom band:
558 exon 4-excluded YAP1 mRNA. **f)** Venn diagram representation of the common transcripts identified as hnRNPC targets
559 by hnRNPC iCLIP-seq data that were also found differentially spliced (AS events) in hnRNPC KD in NHDF cells. **g)** GO
560 network representation of the RNA targets of hnRNPC displaying altered splicing upon hnRNPC silencing and
561 belonging to Hippo signaling Pathway (HSA04390). **h)** Sashimi plot depicting YAP1 skipped exon (SE) AS event (exon 4)
562 in hnRNPC KD NHDFs (red) and controls (orange). The exon inclusion level (IncLevel) is indicated. **i)** Genome browser
563 view of YAP1 gene displaying the iCLIP data (crosslink events per nucleotide) of hnRNP C (blue) (average of N = 3) in
564 proximity of exon 4.
565
566
567 **hnRNPC regulates the AS of genes involved in cardiovascular diseases**
568 We next used our iCLIP and alternative splicing analyses to validate the RNA-IP results obtained in
569 the diseased human heart **(Fig. 4).** We figured this approach might help us unveil the direct targets
570 of hnRNPC in the pathological heart, where the RBP levels and localization are perturbed **(Fig. 1c,**
571 **d; Fig. 3a, b).** We matched the three datasets to identify 389 common transcripts which are
572 physically bound by hnRNPC in the failing hearts and undergo alternative splicing in its absence
573 (**Fig. 8a; Supplementary Data 8**). Among them, we again confirmed the presence of the
574 components of the Hippo pathway (**Supplementary Data 6**).
575
576 The Comparative Toxicogenomics Database (CTD) annotation of the transcripts targeted for gene–
577 disease associations yielded cardiovascular, cancer and neurological diseases as the main
578 represented categories (**Fig. 8b; Supplementary Data 8**). In particular, 41 hnRNPC direct targets
579 belonging to the cardiovascular disease category displayed AS in hnRNPC KD cells (**Fig. 8c;**
580 **Supplementary Data 8**). We confirmed the importance of hnRNPC depletion in exon inclusion by
581 visualizing the splice junction of selected transcripts belonging to this category and by highlighting
582 hnRNPC binding sites on those transcripts (**Fig. 8d, e**).
583 Next, we investigated whether the splicing events determined by hnRNPC depletion *in vitro* are
584 relevant in HF. Hence, we analysed YAP1 exon 4 splicing in our cohort of patients diagnosed with
585 HF and found an increase in exon 4 inclusion in the majority of the samples considered
586 (**Supplementary Fig. 11a**). The variability of this result is expected due to the intrinsic complexity
587 of the cardiac tissue (i.e.: heterogeneous cellular composition of the failing human heart, the
588 presence of fibrotic tissue).
589

590 We then adopted the MATs statistical algorithm to quantify the changes in YAP1 exon 4 AS in RNA-
591 seq datasets obtained from patients diagnosed with heart failure and previously published
592 (GSE108157 and GSE141910). Here, we confirmed that failing human hearts display a higher
593 inclusion of exon 4 in *YAP1* transcript, thus supporting our data (**Supplementary Fig. 11b**).
594 Finally, we used the same RNA-seq datasets to further corroborate the clinical relevance of the AS
595 events affected by hnRNPC depletion on a larger scale and found that numerous AS events
596 determined by hnRNPC KD in NHDFs also occurred in the failing heart, independently of the
597 etiology of the pathology (**Supplementary Fig.11c**; **Supplementary Data 9**).
598
599 Taken together, these results indicate that pathological ECM remodeling in the failing heart
600 induces hnRNPC shuttling to the sarcomeres, where the RBP localizes in close proximity to the
601 translation apparatus. A reduction in hnRNPC nuclear localization and in its contribution to the
602 splicing process affects the AS of mechanosensitive transcripts and RNAs involved in
603 cardiovascular diseases.

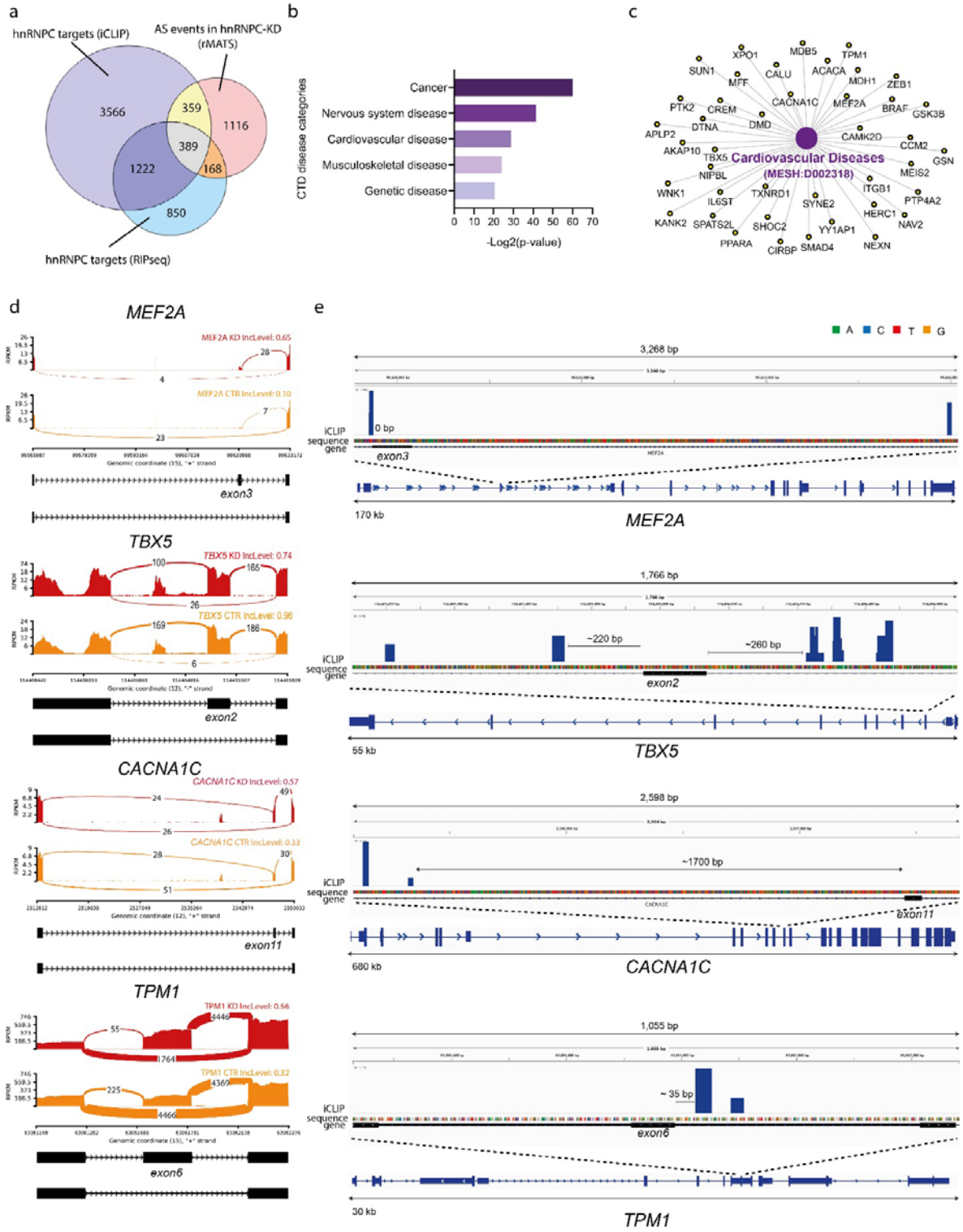

Figure 8. hnRNPC regulates AS of genes involved in cardiovascular diseases. a) Venn diagram representation of the transcripts common to the following datasets: iCLIP-seq in NHDFs, RNAseq AS-analysis in hnRNPC KD NHDF and hnRNPC RNA-IP in failing human hearts. **b)** Gene Ontology (GO) analysis of the 389 transcripts common to the three datasets as obtained by Comparative Toxicogenomics Database (CTD). **c)** GO network representation of the transcripts

610 belonging to Cardiovascular Disease (MESH: D002318) category and common to the three datasets analyzed: iCLIP-
611 seq, AS (rMATS) in *HNRNPC* KD NHDF and hnRNPC RNA-IP in failing human hearts. **d)** Sashimi plots depicting
612 representative skipped exon AS events in *MEF2A*; *TBX5*; *CACNA1C* and *TPM1* belonging to Cardiovascular Disease
613 category of the CTD database in hnRNPC KD NHDFs (red) and controls (orange). The exon inclusion level (IncLevel) is
614 indicated. **e)** Genome browser view of individual genes displaying the iCLIP data (crosslink events per nucleotide) of
615 hnRNP C (blue) (average of N = 3) in proximity of specific exons. See also **Supplementary Data 6-8**.
616

617 **DISCUSSION**

618 Cardiac pathologies are characterized by a profound modification of the composition and
619 mechanics of the local ECM — a phenomenon referred to as ventricular remodeling. This process
620 impairs cardiomyocyte contractility and thus contributes to the progressive deterioration of heart
621 function [5]. The active cardiomyocyte response to ventricular remodeling is considered as a
622 compensatory mechanism that aims to minimize the detrimental effects of the increased
623 biomechanical stress on cardiac output, while protecting the integrity and the pumping activity of
624 the organ [59].
625
626 Here we performed an *in silico* analysis of published expression profiling array datasets obtained
627 from ischemic and non-ischemic heart, with the aim of identifying molecular mediators that help
628 ensure cell adaptation to the new demands of the pathological organ by reshaping gene
629 expression. We observed a general upregulation of RBP expression in the pathological heart in
630 humans and in mice, independently of the etiology of the pathology. We identified hnRNPC among
631 the RBPs consistently altered in the diseased heart; the upregulation of this abundant nuclear
632 protein, which has so far mainly been studied for its role as a splicing factor [28–30], has been
633 independently confirmed by single cell RNA sequencing in cardiomyocytes [34]. The upregulation is
634 more pronounced at the protein level, suggesting post-transcriptional processes might be at play
635 in order to increase protein stability.
636
637 We took hnRNPC forward for further analyses – employing quantitative proteomics, super-
638 resolution microscopy and PLA to disclose that hnRNPC shuttles out of the nucleus and localizes to
639 the sarcomeres of cardiomyocytes in the pathological heart. We confirmed this observation by
640 biochemical analyses, and found that the protein settles at the Z-disc, where it physically interacts
641 with components of the contractile apparatus, including Troponin T2, PDLIM5, FHL2 and MYH7.
642
643 hnRNPC upregulation has been associated with different pathologies, including atherosclerosis
644 and pre-atherosclerotic intimal hyperplasia [33], neurodegenerative diseases [31] and some forms of
645 cancer (e.g. gastric cancer) [60]; however, modifications in its localized function have not been
646 described in pathological conditions. Indeed, most hnRNPs shuttle between the nucleus and the
647 cytoplasm; hence their interaction with specific binding partners can be considered as an indicator

648 of their function at specific cell compartments. Interestingly, in chemoresistant gastric cancer,
649 hnRNPC was found upregulated and localized to the cytoplasm and membrane, but its function in
650 these compartments was not questioned [60]. Our mass spectrometry analysis of hnRNPC-
651 interacting proteins in diseased human heart samples confirmed that hnRNPC protein interacts
652 with the spliceosome, as previously demonstrated [61]. However, the presence of spliceosome
653 components was reduced in hnRNPC interactome in failing hearts compared to healthy hearts.
654 Interestingly, the presence of proteins belonging to the cytoskeleton, the sarcomere and the
655 ribosome specifically in the failing heart interactome suggested a different function for hnRNPC in
656 diseased conditions.

657 To determine what this new function might be, we performed RIP-seq and identified several
658 specific exon-enriched hnRNPC-bound RNAs in the failing heart, mostly encoding for sarcomeric
659 proteins. Some of these mRNAs, including titin (*TTN*), cardiac muscle alpha actin (*ACTC1*) and
660 cardiac troponin I3 (*TNNI3*) are translated locally at the sarcomeric site [42,43]. Together with the
661 evidence that hnRNPC interacts with ribosomal proteins at the sarcomere, these data led us to
662 hypothesize that hnRNPC shuttling to the contractile apparatus in the failing heart could be
663 associated with the localized translation of transcripts encoding for contractile proteins.

664 Localized translation has been described in different cell types, including neurons [62], fibroblasts [63]
665 and myoblasts [64], as a strategy aimed at maximizing the synthesis of needed proteins directly at
666 the site of exploitation. Indeed, hnRNPC was previously found in RNA granules in neurons together
667 with mRNAs involved in synaptic remodeling, which are transported to the subsynaptic site and
668 translated in response to an input [65]. Sarcomeres serve as sites of active translation in the rat
669 heart, where the translation machinery and mRNAs encoding for sarcomeric proteins are
670 distributed in a cross-striated pattern [43]. We used iPSC-derived cardiomyocytes to visualize the
671 active incorporation of PMY (an indicator of active translation) at the sarcomere, where ribosome
672 components are found. By coupling decellularized extracellular matrices obtained from healthy
673 and diseased human hearts with ribopuromycilation and PLA, we found that the pathological ECM
674 induces hnRNPC recruitment to the sarcomeric active sites of translation.

675 Because cardiac ECM remodeling is associated with mechanical stress, we used 3D hydrogels with
676 controlled stiffness and micropatterned surfaces to demonstrate that a fraction of hnRNPC can
677 shuttle outside of the nucleus when the transmission of intracellular tension is hindered. We

678 confirmed that its shuttling to the cytoplasm is precipitated in constrained cells not able to
679 propagate intracellular tension. It thus seems that the mechanical stress associated with ECM
680 remodeling serves as a switch for hnRNPC redistribution from the nucleus to the sarcomere,
681 presumably to modulate its role in RNA homeostasis. Given hnRNPC shuttling out of the nucleus
682 and its reduced interaction with spliceosomal components, we investigated the effect of hnRNPC
683 depletion on pre-mRNAs AS. To mimic a situation in which hnRNPC function in splicing is reduced,
684 we induced its shuttling from the nucleus by pharmacological inhibitors of tension in NHDFs,
685 which are known to be extremely sensitive to mechanical cues. Together with the results obtained
686 by hnRNPC knock down in the same cell type and iPSC-derived cardiomyocytes, these experiments
687 indicate hnRNPC depletion from the nucleus affects the AS of mechanosensitive transcripts and
688 genes involved in cardiovascular diseases. Next, we used iCLIP-seq to confirm the presence among
689 hnRNPC direct targets of components of the Hippo pathway, a molecular axis involved in
690 organogenesis and whose dysregulation has been associated to numerous pathologies [66],
691 including those affecting the heart [22,52,55,67]. In particular, we found that the mechanically induced
692 hnRNPC displacement from the cell nucleus or its depletion affect the inclusion of YAP1 exon 4.
693 This splicing event is of particular relevance, since the exon encodes for the second WW domain, a
694 domain known to directly control the protein interaction with TEAD transcription factor and thus
695 its DNA binding activity [49]. This switch towards the expression of YAP1 isoforms with two WW
696 domains (YAP1-2) has been recently described by our research group in human pathological hearts
697 [56] and confirmed in other two independently published RNA-seq datasets.
698 Going forward, questions remain as to which upstream factors are involved in hnRNPC regulation
699 in failing hearts and what is the specific role of hnRNPC at the translation sites
700 (repressor/activator).
701 Indeed, although our data suggest an involvement of hnRNPC in localized translation at the
702 sarcomeric site in HF, future work is needed to elucidate whether hnRNPC plays a direct role in
703 this process and its relevance in the establishment and progression of cardiac diseases.
704 The presence of the hnRNPC transcript in our RIP- and iCLIP-seq analyses suggests that hnRNPC
705 could regulate its own RNA post-transcriptionally. RBPs were previously proposed to bind and
706 regulate the fate of their transcripts in an autoregulatory feedback [68]. Further studies are thus
707 needed to elucidate whether hnRNPC adopts this mechanism to regulate its expression and
708 function in cardiac pathologies.

709 In conclusion, our results on the regulation of hnRNPC localization and function unveil a novel
710 mechanism by which RNA homeostasis could undergo mechanical regulation following
711 pathological cardiac ECM remodeling (**Fig. 9**). Future experiments that study the mechanical
712 control of RNA homeostasis and the players involved are now warranted, as the ability of RNA
713 binding proteins (RBPs) to serve as possible mechanosensors could explain how ECM mechanics
714 can directly affect cell differentiation and function by controlling RNA fate in a stage-specific
715 manner.

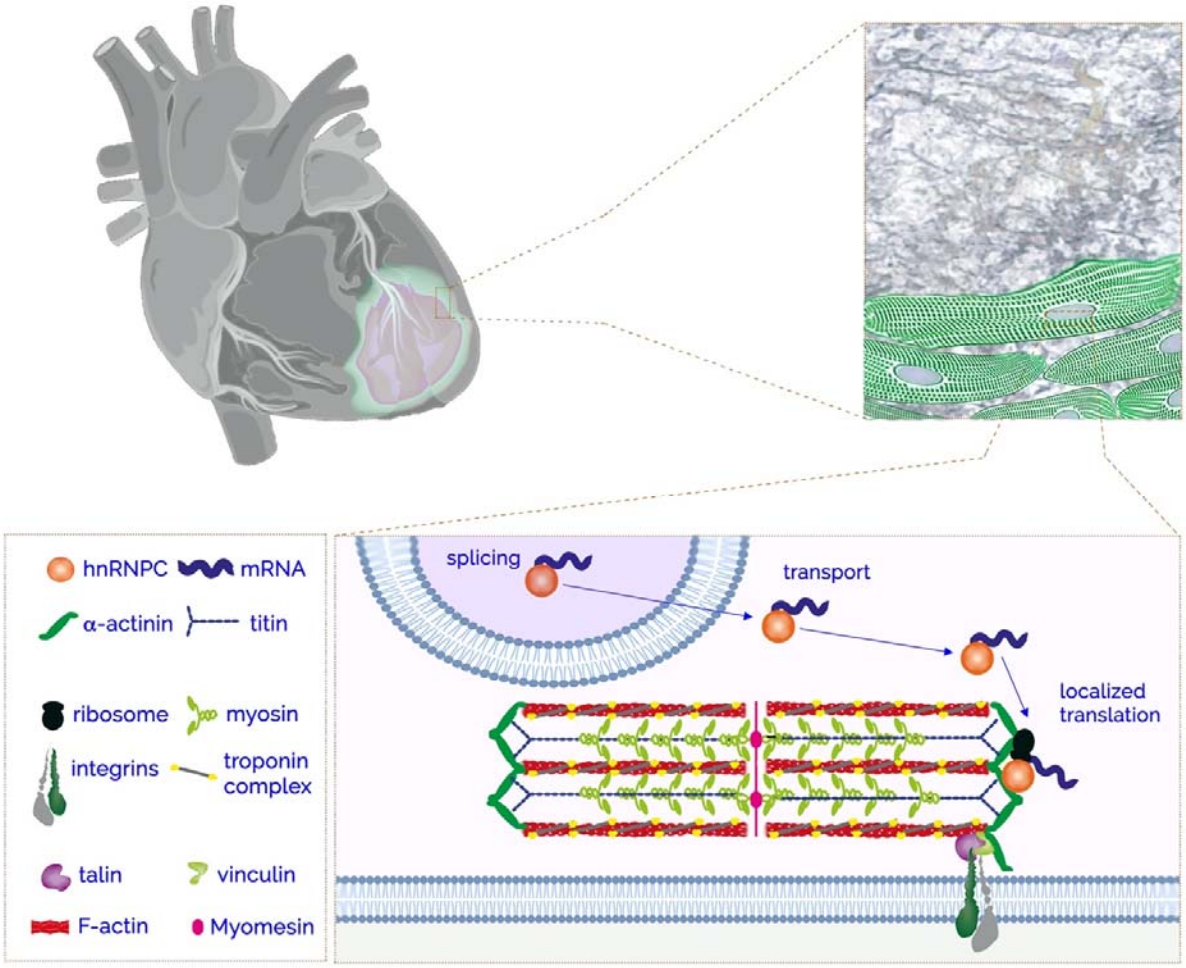

716

717 **Figure 9: Graphical representation of hnRNPC displacement in the pathological heart.**

718

719 **Methods**

720 **Study approval**

721 This study was performed in accordance with the ethical standards of the Centre of Cardiovascular
722 and Transplantation Surgery and was approved by the Ethics Committee of St. Anne's University
723 Hospital, Brno, Czech Republic. The experiments were done according to the Declaration of
724 Helsinki (2000) of the World Medical Organization. Experiments involving mice were approved by
725 the Instituto de Biologia Molecular e Celular – Instituto de Engenharia Biomédica (IBMC-INEB)
726 Animal Ethics Committee and the National Direção Geral de Veterinária (permit no: 022793), and
727 conformed with Directive 2010/63/EU of the European Parliament.

728

729 **Patient-derived heart samples**

730 Diseased heart tissue samples (N=17) were obtained from left ventricle of patients diagnosed with
731 end-stage heart failure undergoing cardiac transplantation or ventricular assist device
732 implantation. The classification of ischemic (N = 8) and non-ischemic (N = 9) heart failure is defined
733 based on the patient anamnesis, as per the International Statistical Classification of Diseases and
734 Related Health Problems (ICD-10). Healthy hearts (N=3) obtained from deceased organ donors
735 without a history of cardiac disease were used as a control (**Supplementary Table 1)**.

736

737 **Mouse model of myocardial infarction (MI)**

738 MI was experimentally induced by ligating the left anterior descending coronary artery in
739 C57BL/6 adult mice (9-10 weeks), as previously described [36] (**Supplementary Methods**). Mice
740 hearts cohort was composed of 4 days post-MI (acute MI), 21 days post-MI (chronic MI), sham-
741 operated (no ligation of the coronary artery) (**Supplementary Fig. 3b**). All animal experiments
742 were approved by the local Ethics Committees.

743

744 **Proximity Ligation Assay**

745 The proximity ligation assay (PLA) was performed on fixed (4% PFA) heart tissue slices and cells
746 using DuoLink PLA technology probes and reagents (**Supplementary Table 2**) and following the
747 manufacturer's protocol (**Supplementary Methods**).

748

749 **Ribopuromycilation**

750 Ribopuromycilation protocol (RPM) to visualize active sites of translation was performed following
751 the original RPM protocol – Procedure A[66,67] (**Supplementary Methods**; **Supplementary Fig. 5d**).
752 The RPM experiments were performed on beating cardiomyocytes between days 20 and 30 of
753 differentiation.

754

755 **Cell culture, differentiation, transfection, treatment and micropatterning**

756 Culture of the human induced pluripotent stem cell line DF 19-9-7T (iPSC) (WiCell, Madison, WI,
757 USA) and normal human dermal fibroblasts (NHDF, ATCC) as well as cardiac differentiation is
758 detailed in **Supplementary Methods**. Cardiac troponin T (**Supplementary Table 2**) was used as
759 sarcomeric marker of iPSC-derived cardiomyocytes. Treatment of cells with inhibitors of
760 cytoskeletal tension, 3D cultures in fibrin gels and micropatterning are detailed in **Supplementary**
761 **Methods**.
762 *HNRNPC* knockdown was performed as previously described[27]. Detailed procedures for siRNA
763 transfection, qRT-PCR and western blotting are described in **Supplementary Methods**.

764

765 **Protein Immunoprecipitation (IP)**

766 For the IP of hnRNPC-binding proteins, 100 mg of tissue from the human heart apex was used for
767 each IP and control sample (**Fig. 2a**). The sample was washed in ice-cold PBS, dissected and
768 mechanically homogenized in 1ml of Lysis Buffer using 3.0 mm Zirkonia beads and Beadbug
769 homogenizer. Dynabeads Protein G (50 µl/sample) were incubated with 200 µl primary antibody
770 (5 µg/sample) for 45 min at 4 °C. Heart lysates were incubated with antibody conjugated
771 Dynabeads overnight at 4°C. The proteins were then eluted by incubation with 100 µl 8M Urea on
772 a shaker (20 min at RT). The eluates were then processed for mass spectrometry analysis
773 (**Supplementary Methods; Supplementary Table 2)**.

774

775 **Mass spectrometry**

776 After protein immunoprecipitation, the samples were digested with trypsin using the FASP
777 method. The digested peptides were labeled using TMT pro16-plex isobaric mass tagging reagents
778 (Thermo Scientific) and the fractions were analyzed on an Orbitrap Fusion™ Lumos™ Tribrid™
779 mass spectrometer interfaced with an Easy-nLC1200 liquid chromatography system (Thermo
780 Fisher Scientific). The IP/IgG abundances were calculated for each sample. A protein was

781 considered successfully immunoprecipitated when a ratio > 1.5 was detected in both biological
782 replicates. See also **Supplementary Methods** and **Supplementary Table 2**.
783
784 **RNA Immunoprecipitation (RIP)**
785 To immunoprecipitate hnRNPC-binding RNAs, 100 mg tissue from the human heart apex was used
786 for each IP and control sample. In brief, the heart samples were dissected, cross-linked in 1% (v/v)
787 formaldehyde, mechanically dissociated in 1 ml Polysome Lysis Buffer (PLB) using 3.0 mm Zirkonia
788 beads and a Beadbug homogenizer and sonicated. Dynabeads Protein G (100 µl/sample) were
789 incubated with 10 µg of primary antibody (sc-32308, sc-2025) for 1 h at 4 °C. Cross-linked lysate
790 was incubated with antibody-conjugated Dynabeads overnight at 4°C. Reverse cross-linking was
791 performed and the proteins were digested by incubation with Proteinase K (60 µg/sample) for 1.5
792 h at 55 °C on a shaker. RNA extraction was then performed following standard phenol:chloroform
793 phase separation. The protocol is depicted in **Fig. 4a** and detailed in **Supplementary Methods**.
794
795 **RNA sequencing, RIP-seq and alternative splicing (AS) analysis**
796 A sequencing library was prepared using a NEBNext Ultra II Directional Kit (New England Biolabs,
797 MA, USA). For the RIP-sequencing, the immunoprecipitated RNA was used as an input into the
798 total RNA library preparation protocol; control input RNA was first rRNA depleted using QIAseq
799 Fastselect HMR Kit (Qiagen, Germany). For the alternative splicing analysis, 200-300 ng total RNA
800 was used as an input into the polyA enrichment module protocol. Samples were fragmented and
801 transcribed into cDNA. Following universal adapter ligation, the samples were barcoded using dual
802 indexing primers. The RNA resultant from RIP of heart tissue or resultant from NHDF transfection
803 with hnRNPC siRNA and the respective control construct was sequenced on an Illumina Nextseq
804 550 sequencer (Illumina, CA, USA) to 25-35 million single-end 75bp reads and >50 million paired-
805 end 75 bp reads per sample, respectively. Detailed sequencing procedure and analysis are
806 available in the expanded methods section (**Supplementary Methods; Supplementary Table 2**).

807 **Individual-nucleotide resolution UV crosslinking and immunoprecipitation (iCLIP) of**
808 **hnRNPC1/C2**

809 NHDFs were grown to 85-90% confluency and exposed to 150 mJ/cm2 at 254 nm in a Stratalinker
810 2400 on ice. Cell pellets were resuspended in 1ml of ice-cold lysis buffer (**Supplementary**

811 **Methods**). The insoluble fraction was removed by centrifugation at 20.000g for 20 min at 4°C and
812 the supernatant was used for the iCLIP experiment. Dynabeads Protein G (Invitrogen) (100
813 µl/sample) were incubated with 15 µg of anti HNRNPC1/C2 antibody (Santa Cruz) in a total volume
814 of 100 µl of lysis buffer for 1 h at RT. Antibody coupled beads were mixed with 1ml of soluble cell
815 lysate and incubated for 1hour on a rotator at 4°C. Dephosphorylation, radiolabeling (γ-ATP) and
816 3' end adapter ligation was carried out on the protein-RNA complex. The resultant Protein-RNA
817 complex was resolved on a gradient NuPAGE gel and blotted onto nitrocellulose membrane. Post-
818 autoradiography the membrane was cut between 48-100kDa size and Proteinase K treatment was
819 performed to isolate RNA. The cDNA libraries were prepared as previously described [69] with slight
820 modifications. The purified library was analyzed by 75bp single end high-throughput sequencing at
821 Illumina HiSeq2500. Protocol and reagents are detailed in **Supplementary Methods and**
822 **Supplementary Table 2**. A schematic representation of the protocol can be found in
823 **Supplementary Fig. 7f**.
824
825 **Decellularization of human myocardial tissue and preparation of ECM coating**
826 The decellularization protocol was performed as previously described[23,70] **(Supplementary**
827 **Methods)**. The ECM-enriched scaffold was mechanically disrupted and used as 2D coating for cell
828 culture (**Fig. 5c, d**).
829
830 **Microscopy and image analysis**
831 Histology, immunohistochemistry and immunocytochemistry are detailed in **Supplementary**
832 **Methods**. A Zeiss LSM 780 confocal microscope with 40x (1.3 NA) oil-immersion or 20x air (0.8 NA)
833 objective lenses was used for image acquisition. ImageJ and Imaris software were used for image
834 quantification (**Supplementary Methods**). For the Masson's Trichrome analysis, a slide scanner
835 Zeiss Axio Scan Z1 microscope was used to visualize whole tissues using the bright-field mode and
836 a 10x objective. Super-resolution imaging was performed using a 3D-SIM Deltavision OMX with a
837 60x objective (1.42 NA).
838
839 **Statistical Analyses**
840 All data are expressed as the mean ± standard deviation (S.D.) unless otherwise specified. The
841 statistical analyses were performed by using GraphPad Prism v. 6.0 software package. The null

842 hypothesis was rejected when $P < 0.05$. The number of biological (N) and technical (n) replicates
843 and the statistical tests used are indicated in figure legends and in the Source Data file.

844 **Data Availability**

845 All data supporting the findings of this study are available as Supplementary Data. Sequencing
846 data have been deposited to GEO database under the reference series GSE155474 and
847 GSE169068. The Mass Spectrometry proteomics data have been deposited to the
848 ProteomeXchange Consortium via the PRIDE partner repository under the dataset identifier
849 PXD020663.

850

851 **Acknowledgements**

852 The authors would like to thank Carina Sihlbom and Johannes Fuchs at the Proteomics Core
853 Facility at Sahlgrenska Academy, University of Gothenburg, Sweden for proteomic analysis. They
854 also thank the technical support team at the Center of Translational Medicine, the members of the
855 Mass Spectrometry Core Facility of FNUSA-ICRC, the Core Facility Bioinformatics of CEITEC
856 Masaryk University, the CF Genomics supported by the NCLG research infrastructure (LM2018132
857 funded by MEYS CR), for their assistance with obtaining the scientific data presented in this paper.
858 The authors are grateful to Jessica Tamanini of Insight Editing London for reviewing and editing
859 the manuscript prior to submission and to Jan Vrbsky for primer design. The authors also thank
860 Perpetua Pinto-do-Ó and Diana S Nascimento for providing the mouse model of MI. Super-
861 resolution microscopy was performed at the Materials Characterization and Fabrication Platform
862 (MCFP) at The University of Melbourne.

863 **Sources of Funding**

864 Fabiana Martino was supported by the European Regional Development Fund - Project ENOCH
865 (No. CZ.02.1.01/0.0/0.0/16_019/0000868). Ana Rubina Perestrelo, Giancarlo Forte, Stefania
866 Pagliari were supported by the European Social Fund and European Regional Development Fund-

867 Project MAGNET (CZ.02.1.01/0.0/0.0/15_003/0000492). Frank Caruso acknowledges the award of
868 a National Health and Medical Research Council Senior Principal Research Fellowship
869 (GNT1135806). Francesca Cavalieri acknowledges the award of an Australian Research Council
870 (ARC) Future Fellowship scheme (FT140100873) and the European Union's Horizon 2020 Research
871 and Innovation Program under grant agreement No. 690901 (NANOSUPREMI). Waleed S. Albihlal
872 and Andre P. Gerber were supported by the BBSRC (BB/N008820/1) and a Royal Society Wolfson
873 Research Merit Award (WM170036) to APG. Stepanka Vanacova and Nandan Varadarajan were
874 supported by the Czech Science Foundation (20-19617S) and the institutional support CEITEC 2020
875 (LQ1601). Mary O'Connell was supported by the Ministry of Education, Youth and Sports within
876 programme INTER-COST (LTC18052).

877

878 **Author contributions**

879 FM: Conceptualization, Experimental Design and Execution; ARP: Experimental Execution; VHE:
880 Bioinformatics analysis; NMV, SV: iCLIP-sequencing; HD: Experimental Execution; VHO: human
881 tissue harvesting and patient anamnesis; FC, FCAR: Superresolution microscopy, manuscript
882 drafting; WSA, APG: RNA-IP protocol setting and data interpretation; MAOC: paper
883 conceptualization and drafting; SP, GF: project supervision, paper conceptualization and drafting.

884

885 **Declaration of interests**

886 The authors declare no competing interests.

887

888 **References**

889 1. Smith, L., Cho, S. & Discher, D. E. Mechanosensing of matrix by stem cells: From matrix
890 heterogeneity, contractility, and the nucleus in pore-migration to cardiogenesis and muscle
891 stem cells in vivo. *Semin. Cell Dev. Biol.* **71**, 84–98 (2017).

892 2. Martino, F., Perestrelo, A. R., Vinarský, V., Pagliari, S. & Forte, G. Cellular
893 mechanotransduction: From tension to function. *Front. Physiol.* **9**, 1–21 (2018).

894 3. Kim, H. E. *et al.* Disruption of the myocardial extracellular matrix leads to cardiac
895 dysfunction. *J. Clin. Invest.* **106**, 857–866 (2000).

896 4. Parker, M. W. *et al.* Fibrotic extracellular matrix activates a profibrotic positive feedback
897 loop. *J. Clin. Invest.* **124**, 1622–1635 (2014).

898 5. Spinale, F. G. Myocardial matrix remodeling and the matrix metalloproteinases: Influence
899 on cardiac form and function. *Physiol. Rev.* **87**, 1285–1342 (2007).

900 6. Saucerman, J. J., Tan, P. M., Buchholz, K. S., McCulloch, A. D. & Omens, J. H. Mechanical
901 regulation of gene expression in cardiac myocytes and fibroblasts. *Nat. Rev. Cardiol.* **16**,
902 361–378 (2019).

903 7. Taegtmeyer, H., Sen, S. & Vela, D. Return to the fetal gene program: A suggested metabolic
904 link to gene expression in the heart. *Ann. N. Y. Acad. Sci.* **1188**, 191–198 (2010).

905 8. Papait, R. *et al.* Genome-wide analysis of histone marks identifying an epigenetic signature
906 of promoters and enhancers underlying cardiac hypertrophy. *Proc. Natl. Acad. Sci. U. S. A.*
907 **110**, 20164–20169 (2013).

908 9. Nomura, S. *et al.* Cardiomyocyte gene programs encoding morphological and functional
909 signatures in cardiac hypertrophy and failure. *Nat. Commun.* **9**, 1–17 (2018).

910 10. Olson, E. N. & Schneider, M. D. Sizing up the heart: Development redux in disease. *Genes*
911 *Dev.* **17**, 1937–1956 (2003).

912 11. Gao, C. & Wang, Y. mRNA Metabolism in Cardiac Development and Disease: Life After
913 Transcription. *Physiol. Rev.* **100**, 673–694 (2020).

914 12. Beqqali, A. Alternative splicing in cardiomyopathy. *Biophys. Rev.* **10**, 1061–1071 (2018).

915 13. Geuens, T., Bouhy, D. & Timmerman, V. The hnRNP family: insights into their role in health
916 and disease. *Hum. Genet.* **135**, 851–867 (2016).

917 14. Backlund, M. *et al.* Plasticity of nuclear and cytoplasmic stress responses of RNA-binding
918 proteins. *Nucleic Acids Res.* **48**, 4725–4740 (2020).

919 15. Seo, J. Y. *et al.* Heterogeneous nuclear ribonucleoprotein (hnRNP) L promotes DNA damage-
920 induced cell apoptosis by enhancing the translation of p53. *Oncotarget* **8**, 51108–51122
921 (2017).

922 16. Lechler, M. C. & David, D. C. More stressed out with age? Check your RNA granule
923 aggregation. *Prion* **11**, 313–322 (2017).

924 17. Liu, H. & Tang, L. Mechano-Regulation of Alternative Splicing. *Curr. Genomics* **14**, 49–55
925 (2013).

926 18. Simpson, L. J., Reader, J. S. & Tzima, E. Mechanical Regulation of Protein Translation in the
927 Cardiovascular System. *Front. Cell Dev. Biol.* **8**, 1–13 (2020).

928 19. Wang, T., Hamilla, S., Cam, M., Aranda-Espinoza, H. & Mili, S. Extracellular matrix stiffness
929 and cell contractility control RNA localization to promote cell migration. *Nat. Commun.* **8**,
930 (2017).

931 20. Bordeleau, F. *et al.* Tissue stiffness regulates serine/arginine-rich protein-mediated splicing
932 of the extra domain B-fibronectin isoform in tumors. *Proc. Natl. Acad. Sci. U. S. A.* **112**,
933 8314–8319 (2015).

934 21. Rhee, W. J. *et al.* HuR regulates the expression of stress-sensitive genes and mediates
935 inflammatory response in human umbilical vein endothelial cells. *Proc. Natl. Acad. Sci. U. S.*
936 *A.* **107**, 6858–6863 (2010).

937 22. Heallen, T. *et al.* Hippo Pathway Inhibits Wnt Signaling to Restrain Cardiomyocyte
938 Proliferation and Heart Size. *Science (80-.).* **332**, 458–461 (2011).

939 23. Perestrelo, A. R. *et al.* Multiscale Analysis of Extracellular Matrix Remodeling in the Failing
940 Heart. *Circ. Res.* **128**, 24–38 (2021).

941 24. Harpster, M. H. *et al.* Earliest changes in the left ventricular transcriptome postmyocardial
942 infarction. *Mamm. Genome* **17**, 701–715 (2006).

943 25. Barth, A. S. *et al.* Identification of a Common Gene Expression Signature in Dilated
944 Cardiomyopathy Across Independent Microarray Studies. *J. Am. Coll. Cardiol.* **48**, 1610–1617
945 (2006).

946 26. Colak, D. *et al.* Left ventricular global transcriptional profiling in human end-stage dilated
947 cardiomyopathy. *Genomics* **94**, 20–31 (2009).

948 27. Rowell, J., Koitabashi, N., Kass, D. A. & Barth, A. S. Dynamic gene expression patterns in

949 animal models of early and late heart failure reveal biphasic-bidirectional transcriptional
950 activation of signaling pathways. *Physiol. Genomics* **46**, 779–787 (2014).

951 28. König, J. *et al.* ICLIP reveals the function of hnRNP particles in splicing at individual
952 nucleotide resolution. *Nat. Struct. Mol. Biol.* **17**, 909–915 (2010).

953 29. Zarnack, K. *et al.* Direct competition between hnRNP C and U2AF65 protects the
954 transcriptome from the exonization of Alu elements. *Cell* **152**, 453–466 (2013).

955 30. Zhou, R. *et al.* Concerted effects of heterogeneous nuclear ribonucleoprotein C1/C2 to
956 control vitamin D-directed gene transcription and RNA splicing in human bone cells. *Nucleic*
957 *Acids Res.* **45**, 606–618 (2017).

958 31. Borreca, A., Gironi, K., Amadoro, G. & Ammassari-Teule, M. Opposite Dysregulation of
959 Fragile-X Mental Retardation Protein and Heteronuclear Ribonucleoprotein C Protein
960 Associates with Enhanced APP Translation in Alzheimer Disease. *Mol. Neurobiol.* **53**, 3227–
961 3234 (2016).

962 32. Fischl, H. *et al.* hnRNPC regulates cancer-specific alternative cleavage and polyadenylation
963 profiles. *Nucleic Acids Res.* **47**, 7580–7591 (2019).

964 33. Panchenko, M. P., Silva, N. & Stone, J. R. Up-regulation of a hydrogen peroxide-responsive
965 pre-mRNA binding protein in atherosclerosis and intimal hyperplasia. *Cardiovasc. Pathol.*
966 **18**, 167–172 (2009).

967 34. Gladka, M. M. *et al.* Single-Cell Sequencing of the Healthy and Diseased Heart Reveals
968 Cytoskeleton-Associated Protein 4 as a New Modulator of Fibroblasts Activation. *Circulation*
969 **138**, 166–180 (2018).

970 35. Liebermeister, W. *et al.* Visual account of protein investment in cellular functions. *Proc.*
971 *Natl. Acad. Sci. U. S. A.* **111**, 8488–8493 (2014).

972 36. Nascimento, D. S. *et al.* MIQuant - semi-automation of infarct size assessment in models of
973 cardiac ischemic injury. *PLoS One* **6**, (2011).

974 37. Zhu, Y. *et al.* POSTAR2: Deciphering the post-Transcriptional regulatory logics. *Nucleic Acids*
975 *Res.* **47**, D203–D211 (2019).

976 38. Dvinge, H. Regulation of alternative <scp>mRNA</scp> splicing: old players and new
977 perspectives. *FEBS Lett*. **592**, 2987–3006 (2018).

978 39. Cheng, H. *et al.* Selective deletion of long but not short cypher isoforms leads to late-onset
979 dilated cardiomyopathy. *Hum. Mol. Genet.* **20**, 1751–1762 (2011).

980 40. Guo, W. *et al.* RBM20, a gene for hereditary cardiomyopathy, regulates titin splicing. *Nat.*
981 *Med.* **18**, 766–773 (2012).

982 41. Zhu, C., Chen, Z. & Guo, W. Pre-mRNA mis-splicing of sarcomeric genes in heart failure.
983 *Biochim. Biophys. Acta - Mol. Basis Dis.* **1863**, 2056–2063 (2017).

984 42. Cadar, A. G., Zhong, L., Lin, A., Valenzuela, M. O. & Lim, C. C. Upstream open reading frame
985 in 5′-untranslated region reduces titin mRNA translational efficiency. *Biochem. Biophys.*
986 *Res. Commun.* **453**, 185–191 (2014).

987 43. Lewis, Y. E. *et al.* Localization of transcripts, translation, and degradation for spatiotemporal
988 sarcomere maintenance. *J. Mol. Cell. Cardiol.* **116**, 16–28 (2018).

989 44. Zarnescu, D. C. & Gregorio, C. C. Fragile hearts: New insights into translational control in

990 cardiac muscle. *Trends Cardiovasc. Med.* **23**, 275–281 (2013).

991 45. Larsen, T. H., Hesketh, J. E., Rotevatn, S., Greve, G. & Sætersdal, T. Ribosome distribution in
992 normal and infarcted rat hearts. *Histochem. J.* **26**, 79–89 (1994).

993 46. Lian, X. *et al.* Robust cardiomyocyte differentiation from human pluripotent stem cells via
994 temporal modulation of canonical Wnt signaling. *Proc. Natl. Acad. Sci. U. S. A.* **109**, (2012).

995 47. Sullivan, K. E., Quinn, K. P., Tang, K. M., Georgakoudi, I. & Black, L. D. Extracellular matrix
996 remodeling following myocardial infarction influences the therapeutic potential of
997 mesenchymal stem cells. *Stem Cell Res. Ther.* **5**, 0–15 (2014).

998 48. Dupont, S. *et al.* Role of YAP/TAZ in mechanotransduction. *Nature* **474**, 179–184 (2011).

999 49. Nardone, G. *et al.* YAP regulates cell mechanics by controlling focal adhesion assembly. *Nat.*
1000 *Commun.* **8**, (2017).

1001 50. Oliver-De La Cruz, J. *et al.* Substrate mechanics controls adipogenesis through YAP
1002 phosphorylation by dictating cell spreading. *Biomaterials* **205**, 64–80 (2019).

1003 51. Duong, H., Wu, B. & Tawil, B. Modulation of 3D fibrin matrix stiffness by intrinsic fibrinogen-
1004 thrombin compositions and by extrinsic cellular activity. *Tissue Eng. - Part A* **15**, 1865–1876
1005 (2009).

1006 52. Mosqueira, D. *et al.* Hippo pathway effectors control cardiac progenitor cell fate by acting
1007 as dynamic sensors of substrate mechanics and nanostructure. *ACS Nano* **8**, 2033–2047
1008 (2014).

1009 53. Olson, E. N. & Nordheim, A. Linking actin dynamics and gene transcription to drive cellular

1010 motile functions. *Nat. Rev. Mol. Cell Biol.* **11**, 353–365 (2010).

1011 54. Venables, J. P. *et al.* Multiple and Specific mRNA Processing Targets for the Major Human
1012 hnRNP Proteins. *Mol. Cell. Biol.* **28**, 6033–6043 (2008).

1013 55. Del Re, D. P. *et al.* Yes-associated protein isoform 1 (Yapl) promotes cardiomyocyte survival
1014 and growth to protect against myocardial ischemic injury. *J. Biol. Chem.* **288**, 3977–3988
1015 (2013).

1016 56. Vrbský, J. *et al.* Evidence for discrete modes of YAP1 signaling via mRNA splice isoforms in
1017 development and diseases. *Genomics* 135907 (2021) doi:10.1016/j.ygeno.2021.03.009.

1018 57. Keller, K. E., Kelley, M. J. & Acott, T. S. Extracellular matrix gene alternative splicing by
1019 trabecular meshwork cells in response to mechanical stretching. *Investig. Ophthalmol. Vis.*
1020 *Sci.* **48**, 1164–1172 (2007).

1021 58. Yang, F., Yi, F., Han, X., Du, Q. & Liang, Z. MALAT-1 interacts with hnRNP C in cell cycle
1022 regulation. *FEBS Lett.* **587**, 3175–3181 (2013).

1023 59. Schirone, L. *et al.* A Review of the Molecular Mechanisms Underlying the Development and
1024 Progression of Cardiac Remodeling. *Oxid. Med. Cell. Longev.* **2017**, 1–16 (2017).

1025 60. Huang, H. *et al.* HNRNPC as a candidate biomarker for chemoresistance in gastric cancer.
1026 *Tumor Biol.* **37**, 3527–3534 (2016).

1027 61. Neubauer, G. *et al.* Mass spectrometry and EST-database searching allows characterization
1028 of the multi-protein spliceosome complex. *Nat. Genet.* **20**, 46–50 (1998).

1029 62. Willis, D. E. *et al.* Extracellular stimuli specifically regulate localized levels of individual

1030 neuronal mRNAs. *J. Cell Biol.* **178**, 965–980 (2007).

1031 63. Lawrence, J. B. & Singer, R. H. Intracellular localization of messenger RNAs for cytoskeletal
1032 proteins. *Cell* **45**, 407–415 (1986).

1033 64. Rodriguez, A. J., Shenoy, S. M., Singer, R. H. & Condeelis, J. Visualization of mRNA
1034 translation in living cells. *J. Cell Biol.* **175**, 67–76 (2006).

1035 65. Angenstein, F. *et al.* Proteomic characterization of messenger ribonucleoprotein complexes
1036 bound to nontranslated or translated poly(A) mRNAs in the rat cerebral cortex. *J. Biol.*
1037 *Chem.* **280**, 6496–6503 (2005).

1038 66. Camargo, F. D. *et al.* YAP1 Increases Organ Size and Expands Undifferentiated Progenitor
1039 Cells. *Curr. Biol.* **17**, 2054–2060 (2007).

1040 67. Hou, N. *et al.* Activation of Yap1/Taz signaling in ischemic heart disease and dilated
1041 cardiomyopathy. *Exp. Mol. Pathol.* **103**, 267–275 (2017).

1042 68. Müller-Mcnicoll, M., Rossbach, O., Hui, J. & Medenbach, J. Auto-regulatory feedback by
1043 RNA-binding proteins. *J. Mol. Cell Biol.* **11**, 930–939 (2019).

1044 69. Konig, J. *et al.* iCLIP - Transcriptome-wide Mapping of Protein-RNA Interactions with
1045 Individual Nucleotide Resolution. *J. Vis. Exp.* 2–8 (2011) doi:10.3791/2638.

1046 70. Silva, A. C. *et al.* Three-dimensional scaffolds of fetal decellularized hearts exhibit enhanced
1047 potential to support cardiac cells in comparison to the adult. *Biomaterials* **104**, 52–64
1048 (2016).

1049